INFLUENCE OF KINEMATIC SOIL-STRUCTURE INTERACTION ON STRUCTURAL RESPONSE

by

Tuğçe Tetik

B.S., Civil Engineering, Namık Kemal University, 2011

M.S., Earthquake Engineering, Istanbul Technical University, 2016

Submitted to the Institute for Graduate Studies in
Science and Engineering in partial fulfillment of
the requirements for the degree of
Doctor of Philosophy

Graduate Program in Earthquake Engineering

Boğaziçi University

2024

INFLUENCE OF KINEMATIC SOIL-STRUCTURE INTERACTION ON STRUCTURAL RESPONSE

APPROVED BY:

Prof. Eser Çaktı (Thesis Supervisor)	.....
Prof. Erdal Şafak (Thesis Co-supervisor)	.....
Assoc. Prof. Barlas Özden Çağlayan	.....
Prof. Kadir Güler	.....
Prof. Ufuk Hancılar	.....
Assoc. Prof. Ali Özgün Konca	.....

DATE OF APPROVAL: 30.05.2024

ACKNOWLEDGEMENTS

At the end of my Ph.D. journey, during the thesis and throughout the entire Ph.D. education, I realise there are many people to whom I owe sincere gratitude. First and foremost, I would like to express my sincere gratitude to my supervisors and role models, Prof. Erdal Şafak and Prof. Eser Çaktı. Prof. Şafak's innovative approach, ideas, and guidance have been invaluable to my research and academic growth. I am truly grateful to Prof. Çaktı for her steadfast support whenever I am in need. They have never ceased to be inspiring. I would like to convey my appreciation for my thesis progress and defense committee members who gave me their time and feedback: Assoc. Prof. B. Özden Çağlayan, Prof. Ufuk Hancılar, Prof. Kadir Güler, Assoc. Prof. A. Özgün Konca, and Assist. Prof. Karin Şeşetyan. To the esteemed professors at Boğaziçi University, Kandilli Observatory and Earthquake Research Institute, Earthquake Engineering Department, whose dedication and distinctive approaches have provided me with invaluable experiences for my academic growth during my Ph.D. studies, I extend my heartfelt thanks. I also thank all the colleagues I met during my journey in the department, especially F. S. Malcıoğlu, M. Karakaya, N. M. Çağlar, C. Gülenç, and E. Yıldırım for their friendships, motivating talks and enlightening academic discussions. I would also like to express my special thanks to The Earthquake Engineering Field Investigation Team, which gave me the opportunity to work with valuable professors and experts from universities and industries from different countries, and thanks to Assoc. Prof. G. Tanırcan, who allowed me to work on the Tübitak 1002 project (120M799) by establishing a connection with Middle East Technical University. In expressing my gratitude, I cannot overlook the unfailing support of my family. To my parents, İmran and Hüseyin Tetik, and my sister, Tuğba, their unconditional love and encouragement have been the bedrock of my educational journey. To all these marvelous individuals, I express my most profound appreciation and wish for our continued connection throughout life's journey. This thesis is dedicated to my family and Prof. Şafak for their steadfast support and guidance.

ABSTRACT

INFLUENCE OF KINEMATIC SOIL-STRUCTURE INTERACTION ON STRUCTURAL RESPONSE

The Soil-Structure Interaction (SSI) is a phenomenon that can significantly alter the free field ground motion and, therefore, needs to be considered in the design of structures, especially those founded on soft/weak soils. SSI can be incorporated into the dynamic analysis of structures by implementing foundation impedance functions (FIFs), which provide displacements and/or rotations of the soil-foundation system in terms of unit forces and/or moments applied at the foundation level. As the impedance functions are frequency dependent, the available commercial finite element software, based on the time domain framework, encounters difficulties implementing them. This thesis presents the design of discrete-time domain filters for the frequency-dependent FIFs associated with two selected types of foundation systems considering their geometry, embedment depth, and surrounding soil. The transformation has been obtained using the least squares approximation technique. The correlation between the obtained time domain filters and the actual frequency domain filters has been checked by using R-squared values. The proposed procedure, in which the FIFs act as filters capable of transforming the free field ground motions into the motion of the soil-foundation system, provides an easy way to incorporate SSI into the time-domain dynamic analysis of structures. The examples given also highlight the effect of different frequency content of the ground motion (GM) on the SSI. The results are presented to show the effects of SSI on both the response spectra and the structural response. Foundation input motions (FIMs) are applied to a 5-story building model, and the performance of the building under analysis is compared using free field motion (FFM) and FIM in terms of story displacements, inter-story drifts, top displacement, and base shear using the SAP2000 structural analysis and design program.

ÖZET

KİNEMATİK YAPI-ZEMİN ETKİLEŞİMİNİN YAPISAL TEPKİ ÜZERİNDEKİ ETKİSİ

Zemin-Yapı Etkileşimi (ZYE), serbest saha hareketini önemli ölçüde değiştirebilen ve bu nedenle özellikle yumuşak/zayıf zeminler üzerine inşaa edilmiş yapıların tasarımında dikkate alınması gereken bir olgudur. ZYE, yapıların dinamik analizine, temel empedans fonksiyonları aracılığıyla entegre edilebilir. Bu fonksiyonlar, temel seviyesinde uygulanan birim kuvvetler ve/veya momentler açısından zemin-temel sisteminin deplasmanlarını ve/veya rotasyonlarını belirler. Empedans fonksiyonları frekansa bağlı olduğundan, zaman tanım alanına dayalı mevcut ticari sonlu eleman yazılımları, bunları uygulamakta zorluklarla karşılaşmaktadır. Bu çalışma, geometrileri, derinliği ve etrafını çevreleyen zemini göz önünde bulundurularak seçilen 2 adet temel sistemine ait frekansa bağlı temel empedans fonksiyonları için ayrık zamanlı filtrelerin tasarımını sunmaktadır. Zamana bağlı filtreler, en küçük kareler yöntemi kullanılarak elde edilmiştir. Elde edilen filtreler ile frekansa bağlı filtreler arasındaki korelasyon R-kare değerleri ile kontrol edilmiştir. Önerilen prosedür, temel empedans fonksiyonlarının serbest saha hareketlerini zemin-temel sisteminin hareketine dönüştürebilen filtreler olarak hareket ettiği, yapıların zaman alanındaki dinamik analizine ZYE'yi kolayca entegre etmenin bir yolunu sunmaktadır. Örnek temel uygulamaları, farklı frekans içeriğine sahip yer hareketlerinin ZYE üzerindeki etkisini de vurgulamaktadır. Sonuçlar, ZYE'nin hem tepki spektrumları hem de yapısal tepki üzerindeki etkilerini göstermektedir. Zemin-temel sisteminin hareketi, 5 katlı bir bina modeline uygulanmış ve analiz edilen binanın performansı, SAP2000 yapısal analiz ve tasarım programı kullanılarak kat deplasmanları, katlar arası ötelenmeler, tepe yer değiştirmesi, ve taban kesmeleri açısından incelenmiştir. Aynı analiz, serbest saha hareketi altında da yapılıp sonuçlar karşılaştırılmıştır.

TABLE OF CONTENTS

LIST OF FIGURES

LIST OF TABLES

LIST OF SYMBOLS

a_i	Filter coefficient for the past discrete output values
b_i	Filter coefficient for the input values
B	Half-width of rectangular footing
C	Damping
D	Depth from the ground surface to the bottom of the foundation
E	Elasticity of the material
f_s	Sampling frequency
G	Shear modulus of the soil deposit
H	Thickness of the layered soil media
H_w	Foundation impedance function (time-domain filter)
$\overline{h}$	Effective height of the structure
h_n	Total height of the structure measured from the foundation level
i	Complex number
k	Structural Stiffness
K	Stiffness
$\overline{k}$	Effective Structural Stiffness
K_0	Static Stiffness
$K(\omega)$	Foundation impedance function (frequency-domain filter)
$K_1(\omega)$	Frequency-dependent stiffness properties of the soil-foundation system
$K_2(\omega)$	Frequency-dependent damping properties of the soil-foundation system
K_h	Horizontal stiffness
K_θ	Rotational stiffness
L	Length
$\overline{m}$	Effective mass of structure
m_t	Total mass of structure

m	Number of past outputs
n	Number of past inputs
q	index
R	Radius of the circular foundation slab
R_{jb}	Joyner-Boore distance
R_{epi}	Epicentral distance
T	Fixed-based natural period
$\tilde{T}$	Flexible-based period (the modified natural period)
T_a	Fundamental period of the structure
V_s	Shear wave velocity
$W(\omega)$	Weighting function
x[n]	Input sequence
y[n]	Output sequence
z	Backward shift operator
α_0	Dimensionless frequency
β	Soil hysteretic (internal) damping ratio
γ	Average unit weight of the soil
Δ	Time step
ζ	Structural viscous damping
$\tilde{\zeta}$	Effective flexible-based damping
$\tilde{\zeta}_0$	Foundation damping
μ	Mean
σ	Standard deviation
τ	Time
ν	Poisson's ratio of the soil deposit
ω	Radial frequency
ω_p	Most energetic frequency

LIST OF ACRONYMS/ABBREVIATIONS

AFAD	Disaster and Emergency Management Presidency
DTRF	Discrete-Time Recursive Filter
EW	East-West
FAS	Fourier Amplitude Spectrum
FFM	Free Field Motion
FIF	Foundation Impedance Function
FIM	Foundation Input Motion
FT	Footing Type
GM	Ground Motion
IIR	Infinite Impulse Response
IM	Intensity Measure
PGA	Peak Ground Acceleration
PGD	Peak Ground Displacement
PGV	Peak Ground Velocity
SA	Spectral Acceleration
SDOF	Single Degree of Freedom
SISO	Single-Input Single-Output
SSI	Soil-Structure Interaction
TADAS	Turkish Accelerometric Database and Analysis System
TF	Transfer Function
ZYE	Zemin Yapı Etkileşimi

1. INTRODUCTION

The Soil-Structure Interaction (SSI) refers to the influence of the foundation and surrounding soil on the dynamic response of structures. SSI is of crucial importance in the design of resilient structures in earthquake-prone regions, as it influences the response of structures to seismic events. Experts can predict and recommend measures to mitigate potential damage by analysing the interaction between a structure's foundation and the underlying soil. Further research and advancements in SSI can lead to more resilient and secure engineering solutions. The dynamics of SSI are influenced by a number of complex physical processes, including the geometry of the structure and its foundation, the mechanical properties of the soil, and the characteristics of seismic waves. Recent advancements in computational methods and modelling have enhanced the ability to simulate the behaviour of soil-structure systems under seismic loading. These advancements have also led to better construction practices and the development of innovative materials that can withstand earthquake forces, thereby reducing risks to both the buildings and their occupants.

The three critical effects of SSI on structural response are that it increases the fundamental vibration period of the structure, it filters the high frequencies in free-field motions, and it increases the damping. Numerous studies have investigated both analytical and numerical methods for SSI assessment. These methods have provided direct (considering the integrity of the SSI system) and/or substructure (considering the individual components) approximations for assessing SSI. The substructure method is a commonly used approach for evaluating SSI by analysing both kinematic and inertial interaction. Kinematic SSI effects result in deviations of foundation-level motions from those in the free-field motions. This is assessed by analyzing a massless foundation and structure to determine the forces transmitted to the structure. Inertial interaction refers to the interaction between the soil-foundation system and the structure due to inertial forces generated during seismic events [1–3].

Standard seismic structural analysis typically assumes that the ground surrounding a structure's foundation is rigid, and that the foundation's movement matches the free-field motion (FFM), causing vibrations in the superstructure. However, the seismic response of buildings on soft soil can be influenced by the interaction between soil, foundation, and structure, leading to modifications in their dynamic behaviour. A comprehensive understanding of SSI can provide valuable insights into the distinctive seismic response of buildings on soft soils, and form the basis for developing more efficient and resilient seismic design methods. SSI has the ability to increase or decrease the intensity of FFMs depending on the soil and foundation properties. Previous research [1, 4, 5] has highlighted the significance and complexity of this interaction.

The foundation input motion (FIM), which becomes different than the FFM due to SSI, significantly changes the dynamic response of the structure (see Figure 1.1). To obtain FIM, the FFM should be modified by using filters that account for the properties of the foundation and the surrounding soil (Equation (1.1)). These filters change the amplitude and the phase (i.e. damping) of the FFM and are directly related to the inverse of the foundation impedance functions (FIF). Equation (1.2) defines $K(\omega)$ as the foundation impedance function (FIF), which comprises the frequency-dependent stiffness $K_1(\omega)$ and damping $K_2(\omega)$ properties of the soil-foundation system (see Figure 1.2). K_0 represents the static stiffness, which relies on the shear modulus (G) and Poisson's ratio (ν) of the medium.

SSI can be incorporated into the dynamic analysis framework using FIF, which explains how a foundation responds to a unit force and/or moment. FIFs are dependent on the properties of the foundation system, such as its geometry (circular, square, rectangular, strip, arbitrary) and embedment depth (surface, embedded), the direction of the applied load (horizontal, vertical, rotational), the soil environment (homogenous, layered), and they are associated with a rigid massless foundation. Multiple authors have analysed the impact of foundation embedding [6–11], foundation geometry [12–17], and soil characteristics. The influence of SSI can be studied by implementing finite element modeling of soil [18, 19] and foundation, identifying permeable and virtual

boundaries, and examining the impacts of soil expansion and liquefaction [20]. In addition, SSI effects on the eccentricity and torsional behaviour of different buildings have been carried out [21,22]. In brief, many studies have been conducted on theoretical models and experimental investigations [23].

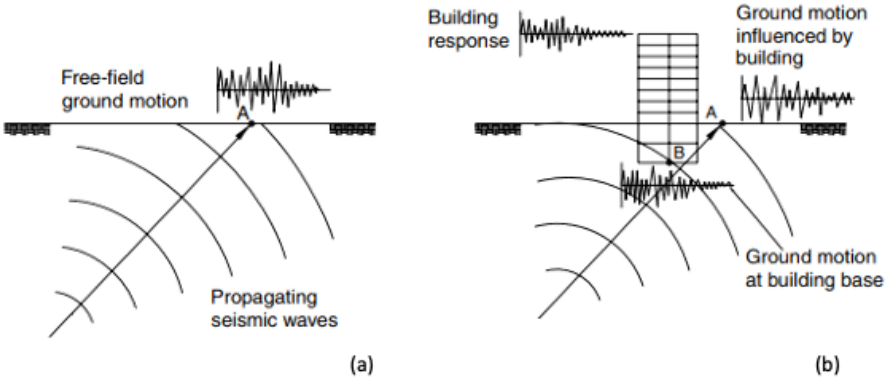

Figure 1.1. Schematic representation of ground motion in the (a) absence and (b) presence of a structure [24].

$$F(t,\omega) = K(\omega)u(t) \tag{1.1}$$

$$K(\omega) = K_0[K_1(\omega) + iK_2(\omega)] \tag{1.2}$$

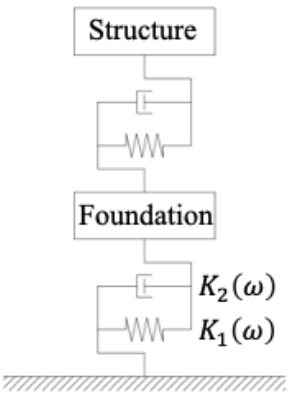

Figure 1.2. Soil-foundation-structure system.

The simplified approach, commonly referenced in recent literature addressing practical challenges in structural dynamics with SSI, was employed to validate and/or compare the results obtained from the transfer function (TF) method [25]. This was done after acknowledging the shortcomings of using a rigid base assumption. This

method simplifies complex computational procedures using a system represented by a simple oscillator that is viscously damped. Its objective is to determine the flexible-based period and damping values.

Veletsos and Meek (1974) proposed that the flexible-based period can be calculated by Equation (1.3) and the fixed-based period is given by the well-known Equation (1.4) [1]. After that, Veletsos and Nair (1975) found the damping relationship, which is shown in Equation (1.5), between fixed-based and flexible-based systems [26].

$$\widetilde{T} = T\sqrt{1+\frac{\overline{k}}{k_h}\left(1+\frac{k_h\overline{h}^2}{k_\theta}\right)} \tag{1.3}$$

$$T = 2\pi\sqrt{\frac{m}{k}} \tag{1.4}$$

$$\widetilde{\zeta} = \widetilde{\zeta}_0 + \frac{\zeta}{\left(\frac{\widetilde{T}}{T}\right)^3} \tag{1.5}$$

where, T, $\widetilde{T}$, $\overline{k}$, k_h, k_θ, $\overline{h}$, m, ζ, $\widetilde{\zeta}$, $\widetilde{\zeta}_0$ are the fixed-based natural period, the flexible-based period (the modified natural period), the structural stiffness, the horizontal stiffness of foundation, the rocking stiffness of foundation, the height of structure, the mass of structure, the structural viscous damping, the effective flexible-based damping, the foundation damping, respectively. In these cases, the fixed-based structural and foundation damping are assumed to be 5%. In Equation (1.3), k_h and k_θ equal to the multiplication of static stiffness and dimensionless frequency.

The fundamental period Equation (1.6) is calculated by the constants C_r and x (related to the structural system), which are provided by the code (BSSC, 2004) [27].

$$T_\alpha = C_r\ h_n^\chi \tag{1.6}$$

$$\omega = \frac{2\pi}{T_\alpha} \tag{1.7}$$

$$\overline{h} = 0.7h_n \tag{1.8}$$

$$\overline{m} = 0.7m_t \tag{1.9}$$

$$\overline{k} = \frac{4\pi^2 \overline{m}}{T_\alpha^2} \tag{1.10}$$

where, h_n, ω, $\overline{h}$, $\overline{m}$, $\overline{k}$, m_t is the total height of the structure measured from the foundation level, the natural frequency of the structure, the effective height, the effective mass, the structural stiffness (Equation (1.7)), and the total mass, respectively. The structure's effective height and mass are considered as 70% of their total values (Equation (1.8) and Equation (1.9)) as stated by BSSC 2004 [27].

In the context of these formulations, Figure 1.3 illustrates how changing the natural period of a structure and modifying the foundation damping influences the design spectral accelerations.

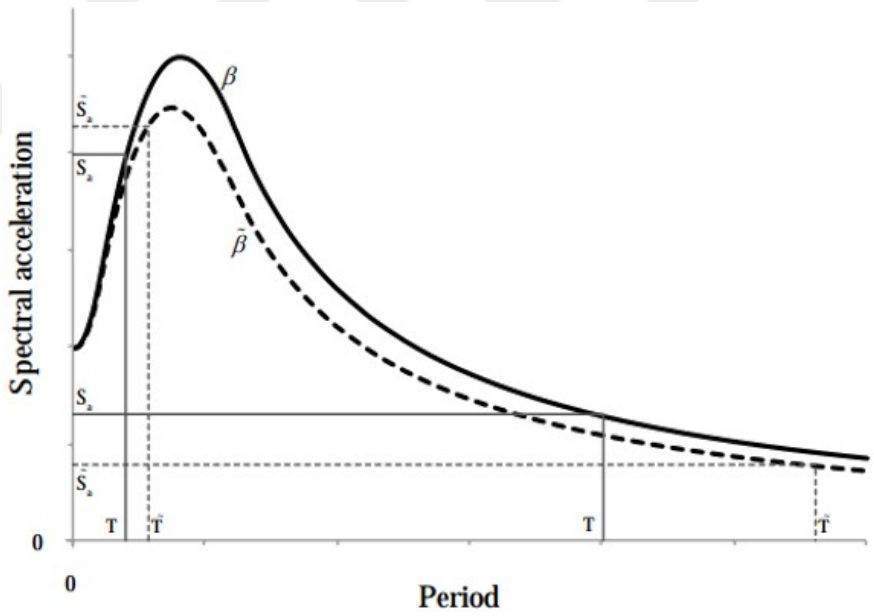

Figure 1.3. Diagram illustrating the impact of period elongation and foundation damping on the design spectral accelerations (The dashed line represents the effects with SSI included, while the solid line shows the effects without SSI) [28].

Previous research using the simplified approach assumes reduced forces in structures due to SSI [29]. At the same time, Mylonakis and Gazetas (2000) emphasize that

the simplified approach may not always reflect reality, and that simplification may lead to unsafe design [30].

The frequency-dependent FIF characterizes the complex response of soils to dynamic loading, including the effects of soil stiffness and damping, and foundation geometry. Various alternative approaches to account for SSI by using frequency-dependent FIFs have been proposed in the literature. However, the frequency dependence of FIF [31] poses difficulties in integrating it into conventional time-domain dynamic analysis software for commercial use. In addition, this frequency domain solution is only applicable to linear analysis and is ineffective for calculating inelastic deformations.

Şafak [32] introduced a novel technique to convert FIFs into filters into discrete-time domain filters, thereby allowing them to be incorporated in standard time-history analysis software. The method is based on the least-squares approximation of frequency-dependent impedance functions by ratios of complex polynomials, which are the spectral representation of discrete-time recursive filters. The background to this method was introduced in the work of Wolf and Motosaka [33].

Following the Şafak's technique, the stability of the filter has been investigated analytically and numerically by other authors. Laudon et al. [34] employed this technique to adjust the frequency response function, and noted that the method suffers from instability despite ensuring accurate identification results. Actually, Şafak [32] also discusses stability problems, and proposes solutions such as checking the placement of the filter poles to ensure they are inside a unit circle in the complex plane, using a weighting function, and adjusting model orders. Gash et al. [35] combined the rational functions with the time-stepping method, meanly Newmark-β method, and found that it does not ensure stability. Lastly, Tang et al. [36] identified stable parameters for rational approximation of single degree of freedom (SDOF) frequency response functions in a semi-infinite medium. They proposed a more accurate and efficient approach by transforming the rational function into partial fractions, and establishing the stability parameter range in this revised format. This ensured both stability and accuracy. The

study suggests that this method provides better computational efficiency compared to previous methods.

Recently, Sung and Chen [37] employed the least-squares method to determine the foundation impedance and studied how soil-structure interaction impacts a SDOF structure. The study demonstrated that ignoring SSI overestimated structural displacement for shorter-period structures and underestimates displacement for longer-period structures.

This thesis proposes the incorporation of SSI into time-domain dynamic structural analysis software, such as the SAP2000 Structural Analysis and Design Program, and illustrates a comparison of spectral acceleration values between two real earthquake records, highlighting the higher values that are significant for understanding structural vulnerabilities. The results are compared using two different foundation types. The investigation mainly aims to provide a deeper understanding of integrating the time domain FIF into the analytical framework.

Engineers can simplify their work by converting frequency-dependent foundation impedance functions into time-domain representations rather than using conventional or simplified methods, and integrating them into SAP2000's time history analysis. However, due to recursive nature of the filter, they have to save some of the past values of input and output during the analysis. This approach can improve the accuracy of the analysis.

The thesis is organized into two primary chapters - Chapter 2 and Chapter 3. Chapter 2 outlines the methodology for transforming discrete-time recursive filters. Chapter 3 examines case studies that investigates the SSI effects on response spectra and structural response for particular foundation forms, considering their geometry, embedment depth, and environmental soil. These examples also highlight the distinction between low-frequency and high-frequency content of ground motion (GM) on SSI. FIMs are obtained for simple FFMs, as well as real earthquake records. First,

the effects of SSI are investigated on response spectra. Then, the effects on a 5-story building model are investigated. The performance of the building under analysis is compared using FFM and FIM in terms of story displacements, inter-story drifts, top displacement, base shear, and story shears utilizing the SAP2000 program.

2. METHODOLOGY

2.1. Discrete-Time Recursive Filters and Estimation of Filter Coefficients

In the field of earthquake engineering, the integration of frequency-dependent foundation impedance functions (FIFs) into conventional time-domain dynamic analysis software poses challenges for commercial applications. Şafak's innovative technique addresses this issue, as well as site amplification problems, by transforming these functions into discrete-time domain filters [32, 38, 39]. This section explores the estimation of coefficients for discrete-time recursive filters, allowing for their straightforward incorporation into time-domain analysis.

A discrete-time filter is a mathematical operator that takes an input sequence x[z] of values and produces an output sequence y[z] as delineated in Equation (2.1) and visualized in Figure 2.1. Their rational value, T, is expressed as the system transfer operator, and its working principle is to contain a recursive relationship between the input and output signals. In this process, the output at each index is determined from the past outputs, and past and present inputs [40].

$$y[z] = Tx[z] \tag{2.1}$$

Figure 2.1. A discrete-time system; a transformation that links an input sequence x[z] to an output sequence y[z] (sketch adapted from [40])

In this context, the discrete-time recursive filters (DTRF) in signal processing comprise three essential elements: the input signal, output signal, and filter coefficients. Filters of this form known as Infinite Impulse Response (IIR) filters, because

they can respond to an impulse indefinitely. The linear difference equation, Equation (2.2), demonstrates the detailed mathematical representation of discretization for the continuous single-input single-output (SISO) linear system.

$$\begin{aligned} y(t) = -a_1 y(t-1) - a_2 y(t-2) - \cdots - a_m y(t-m) + b_0 x(t) \\ + b_1 x(t-1) + b_2 x(t-2) + \cdots + b_n x(t-n) \end{aligned} \tag{2.2}$$

where y(t) and x(t) represent the output and input at time t, respectively. "a_i" refers to the filter coefficient for the past discrete output values, and "b_i" represents the filter coefficient for the input excitations. "m" and "n" denote the number of past outputs and inputs considered, respectively. The filter order controls the input and output signal relationship by assigning weights between the input and output values from $t-1$ to $t-m$ and $t-n$, respectively. Depending on the systems under consideration, the relationships between variables may be linear and time-invariant (if the values of a and b remain constant over time), or they may exhibit non-linear and time-varying properties (if the values of a and b change over time). The DTRF requires a suitable design to ensure stability (i.e., its output is not diverging over time). Conversely, instability may occur, when the output grows infinitely for a bounded input signal. Thus, the mathematical structure of a system is crucial to analyze and estimate its behaviour [32, 39, 40].

The linear difference Equation (2.2) can be expressed more simply by using the backward shift operator, z, which is equal to $e^{i\omega\Delta}$ (where i is a complex number, ω is a radial frequency, and Δ is the sampling interval) in Equation (2.7).

$$y(t) = T(z)x(t) \tag{2.3}$$

$$y(t) = \frac{B(z)}{A(z)}x(t) \tag{2.4}$$

$$A(z) = 1 + a_1 z^{-1} + a_2 z^{-2} + \ldots + a_m z^{-m} \tag{2.5}$$

$$B(z) = b_0 + b_1 z^{-1} + \ldots + b_n z^{-n} \tag{2.6}$$

$$T(z) = \frac{b_0 + b_1 z^{-1} + \ldots + b_n z^{-n}}{1 + a_1 z^{-1} + a_2 z^{-2} + \ldots + a_m z^{-m}} \tag{2.7}$$

The z-transform serves as the discrete-time equivalent of the Laplace transform, which is used for continuous-time signals. Both transforms have a similar relationship to their corresponding Fourier transform.

Most algorithms for estimating the polynomial coefficients of recursive filters in discrete-time signal processing are based on Levy's method. This method approximates complex curve fitting through the least-squares approach, as cited in the literature [41]. It is a mathematical tool commonly used to fit data, and was employed to design IIR filters in this particular investigation. It quantifies discrepancies between the actual and desired filter responses. It does so by finding the best fit for the given experimental data points through minimizing the weighted sum of the squares of residual terms, given by Equation (2.8).

$$E = \min_{b,a} \sum_{z=1}^{n} W(z)[A(z) - B(z)]^2 \tag{2.8}$$

where W denotes the weighting function.

The accuracy of the fit is higher when the residual sums are smaller, indicating an inverse relationship between the precision of the approximation and the magnitude of the residual.

In this thesis, the objective is to minimize the weighted sum of squared residuals, which quantifies the error between the actual data (frequency-dependent impedance function $K(\omega)$) and the estimated data (time-domain impedance function $H(\omega)$). Therefore, to relate Equation (2.8) to our work, the equation is updated as follows.

$$E = \sum_{\omega} W(\omega) \left[H(\omega) - K(\omega)\right]^2 \tag{2.9}$$

Şafak [32] recommended the use of a Gaussian weighting function (Equation (2.10)) to reduce the impact of higher frequencies in designing filters. According to the Gaussian function, the effect of each data point decreases as its distance from

the curve's center increases, resulting in a reduction of high-frequency noise. When applied to Levy's method, this function improves precision in filtering applications by minimizing the impact of outliers.

$$W(\omega) = \frac{1}{\sigma\sqrt{2\pi}} \exp\left(-\frac{1}{2}\frac{(\omega-\mu)^2}{\sigma^2}\right) \tag{2.10}$$

where μ symbolizes the mean, and σ is the standard deviation. Mean gives the data point's distance from the central point, and standard deviation controls the spread or width of the Gaussian function. Smaller values of σ create faster decay, while larger values result in slower decay.

In this process, the system's stability is evaluated using the z-plane. If the chosen filter parameters are located within the unit circle, the system can be deemed stable; meanwhile, if they are observed outside of the unit circle, the system is deemed unstable. These operations are repeated until stability is achieved. The correlation between K(ω) and H(ω) filters may be measured with the R-squared (R^2) value. The Pearson correlation coefficient of the filters is calculated as Equation (2.11) or Equation (2.12). The matrix of correlation coefficients is given in Equation (2.13). Since K(ω) and H(ω) are always directly related to themselves, the diagonal entries are only one as seen in the Equation (2.14). (R^2) close to one indicates the model explains a substantial proportion of the variability in the dependent variable and indicates a strong correlation. Conversely, a value close to zero indicates the model only explains a small portion of the variability, suggesting a poor fit [42].

$$\rho_{K(\omega),\ H(\omega)} = \frac{1}{N-1}\sum_{i=1}^{N}\left(\frac{K(\omega)_i - \mu_{K(\omega)}}{\sigma_{K(\omega)}}\right)\left(\frac{H(\omega)_i - \mu_{H(\omega)}}{\sigma_{H(\omega)}}\right) \tag{2.11}$$

$$\rho_{K(\omega),\ H(\omega)} = \frac{cov\left(K(\omega), H(\omega)\right)}{\sigma_{K(\omega)}\sigma_{H(\omega)}} \tag{2.12}$$

$$R = \begin{pmatrix} \rho_{K(\omega),K(\omega)} & \rho_{K(\omega),H(\omega)} \\ \rho_{H(\omega),K(\omega)} & \rho_{H(\omega),H(\omega)} \end{pmatrix} \tag{2.13}$$

$$R = \begin{pmatrix} 1 & \rho_{K(\omega),H(\omega)} \\ \rho_{H(\omega),\ K(\omega)} & 1 \end{pmatrix} \tag{2.14}$$

Consequently, the soil-foundation subsystem's inherently frequency-dependent impedance functions can now be approximated rationally to transform into the time-domain. To obtain the FIM, the acceleration/displacement of the FFM in time-domain is multiplied by $1/T(z)$, which is in time-domain (Equation (2.15)). The resulting FIM includes the changes in the frequency content of FFM due to foundation soil and foundation geometry.

The filter parameters identified demonstrate a transformation mechanism, whereby the force applied to a foundation is transformed by the filter into FIM. The foundation assumed to have no mass. Our analysis is confined to examining the influence of the geometry and embedment of the foundation and the soil conditions on the FFM. Due to the absence of foundation mass, this influence only modifies the amplitude and phase of the FFM in a frequency-dependent manner, as expressed by the impedance function parameters K and C, and there is no need to consider the K_0 term specified in Equation (1.2).

$$FIM = \frac{1}{T(z)} FFM \tag{2.15}$$

In physical terms, this transformation involves modifying the Fourier transform of the free-field acceleration using the amplitude and phase spectra of the filter. Such modifications result in a decrease in amplitude at higher frequencies and an increase in phase. It should be noted that these modifications can also be achieved in the frequency domain by simply dividing the Fourier transform of the FFM by the amplitude and phase spectra of the filter, and then applying the inverse Fourier transform to obtain the foundation acceleration. However, filtering in the time domain has been found to be simpler and is therefore recommended in practical applications.

2.2. Designing Discrete-Time Filters in MATLAB Programming Language

The Matlab program [43] was employed in the design of discrete-time filters. The code written combines numerical analysis, data interpolation, and signal processing techniques to characterize the impedance properties of the footing types (FTs) considered.

First, the impedance functions representing the frequency-dependent soil stiffness and damping values for each selected foundation type have been compiled from previous studies and digitized [44]. These functions are mostly developed by using empricial and numerical methods, such as finite element methods, and laboratory tests. The applications range from machine foundations to seismically excited structures. The plots of impedance functions taken from the literature are digitized, interpolated to increase the resolution, and given as input to the program to get the parameters of the equivalent discrete-time filters.

Frequencies are defined around the unit circle from 0 to 2π, Equation (2.16). Equation (2.17) provides the sampling frequency calculated according to Nyquist's theorem, which requires a periodic signal needs to be sampled at a rate greater than twice the signal's highest frequency component.

$$w_d = 2arctan\left(\frac{w}{2f_s}\right) \tag{2.16}$$

$$f_s = 2\frac{w_{\max}}{2\pi} \tag{2.17}$$

Discrete-time filter parameters are identified using the "invfreqz" function (Equation (2.18)). By specifying the filter orders (m and n), it returns the real coefficient vectors b and a, numerator and denominator, of the transfer function K(ω), and the frequency weights using the Gaussian weighting function $W(\omega)$. It is defined that the data has a mean value of zero and a standard deviation that can be modified by the user for the considered FTs. The z-plane plot is then visualized using the "zplane" command to check the stability of the filter. Subsequently, the frequency response

of the digital filter, $H(\omega)$ is obtained using the "freqz" function (Equation (2.19)). The magnitude (Equation (2.20)) and phase (Equation (2.21)) values are obtained for both frequency and time domain filters, using the "abs" and "angle" commands, respectively. After that, a correlation analysis is conducted using "corrcoef" function to compare the time-domain and frequency-domain filters of the magnitude and phase. The code then proceeds to obtain the FIM filtering FFM using the a and b parameters as specified in Equation (2.22).

$$[b, a] = invfreqz(Kw, w_d, n, m, W(\omega)) \tag{2.18}$$

$$H(\omega) = freqz(b, a, \omega_d) \tag{2.19}$$

$$K(\omega) = abs(K(\omega)); H(\omega) = abs(H(\omega)) \tag{2.20}$$

$$K(\omega) = angle(K(\omega)); H(\omega) = angle(H(\omega)) \tag{2.21}$$

$$FIM = filter(a, b, FFM) \tag{2.22}$$

The flowchart for the methodology are given in Figure 2.2 and Figure 2.3.

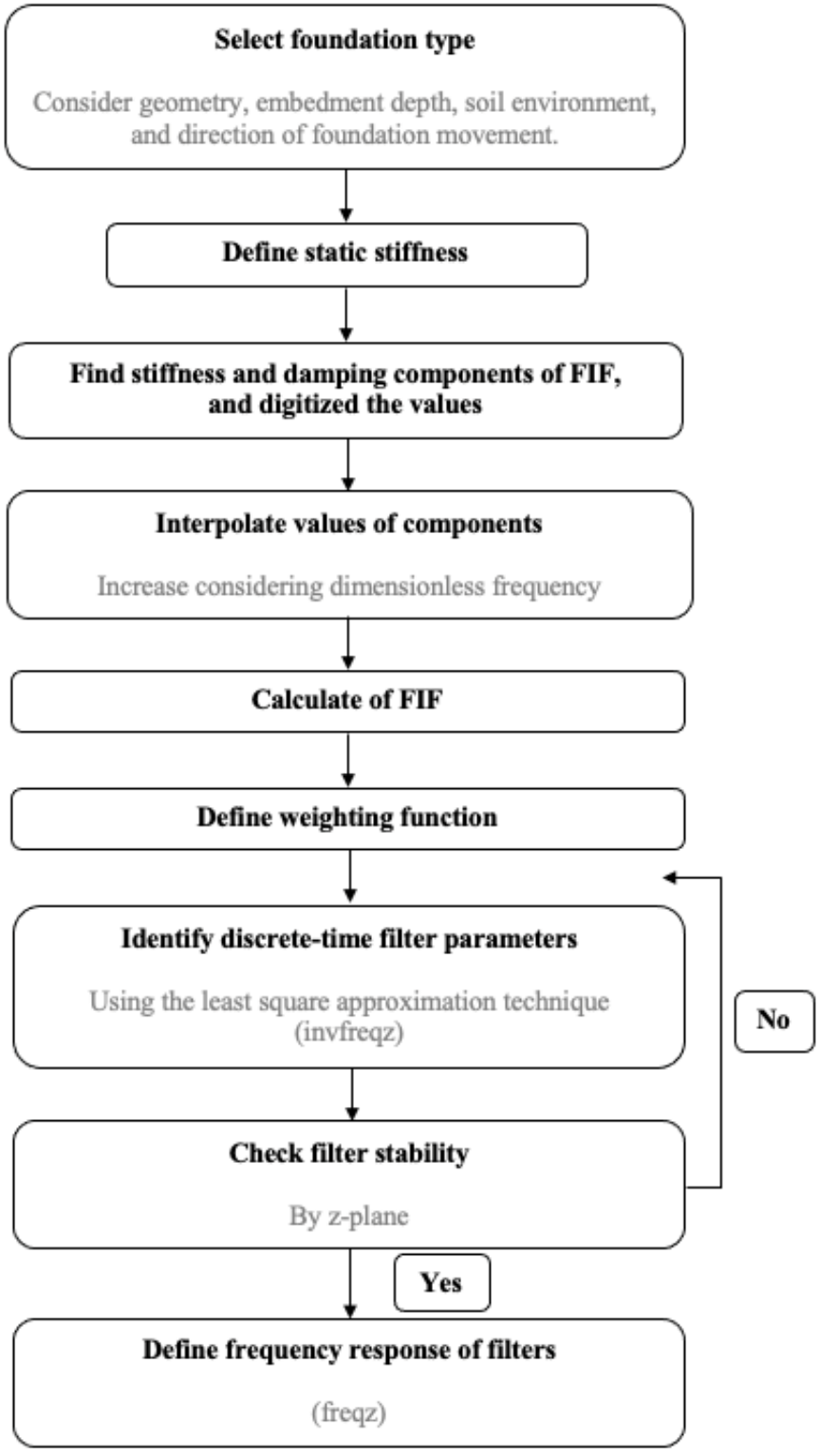

Figure 2.2. The flowchart shows how to design the time domain filters.

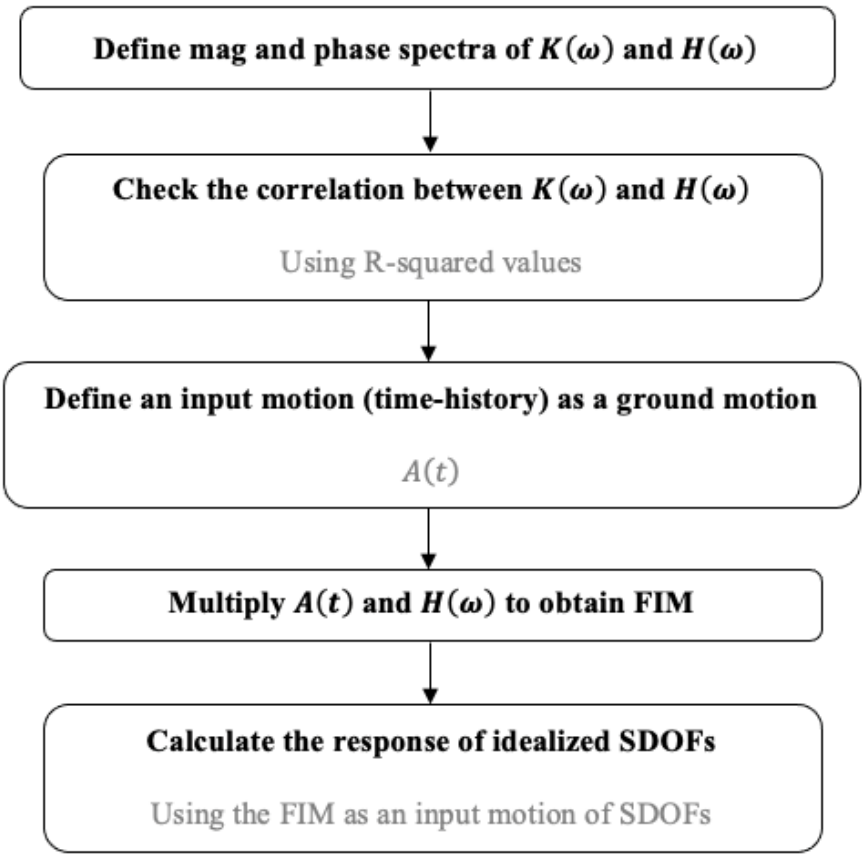

Figure 2.3. The flowchart shows how to use the time domain filters.

3. IMPLEMENTATION OF TIME-DOMAIN FOUNDATION IMPEDANCE FUNCTIONS

3.1. Selection of Free Field Motions

To check the validity of the methodology we considered five types of free-field acceleration time histories: two simulated ones and three real earthquake records. The simulated ones are two Ricker wavelets with different resonance frequencies. The real earthquakes are the accelerations recorded at the three stations during the 6 February 2023 Kahramanmaraş Earthquake. The details are presented below.

3.1.1. Ricker wavelet

To observe the transformation of FFM into FIM and its effect on the response spectrum, we first considered two Ricker wavelets [45]. This helps eliminate processing errors such as baseline corrections and filtering steps. It is crucial for improving the accuracy of the results and enables easy identification and correction of any distortions. Additionally, it simplifies the evaluation of the system's response and overall effectiveness. To compare the effects of SSI on varying frequencies, Ricker-type pulses with 100 Hz sampling rates and resonance frequencies at 0.2 Hz (RW1) and 2.5 Hz (RW2) are created by Equation (3.1) and demonstrated in Figure 3.1. Structures with longer natural periods (such as high-rise buildings, tower structures, suspension bridges, and wind turbines) are less likely to be damaged by low-frequency inputs (e.g., 0.2 Hz Ricker Pulse). On the other hand, shorter, meanly stiffer structures may be more sensitive to higher-frequency inputs (e.g., 2.5 Hz Ricker Pulse).

$$r(\tau) = \left(1 - \frac{1}{2}\omega_p^2\tau^2\right) \exp\left(-\frac{1}{4}\omega_p^2\tau^2\right) \tag{3.1}$$

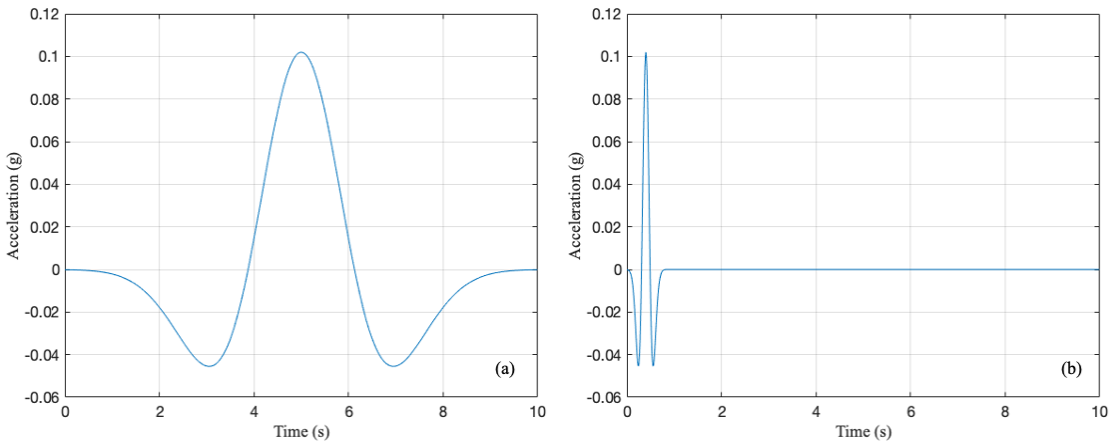

Figure 3.1. Time history of Ricker wavelet; (a) RW1, (b) RW2.

3.1.2. Kahramanmaraş Earthquake (2023)

On 6 February 2023, a series of devastating earthquakes, known as Kahramanmaraş Earthquake Sequence, struck southern and central Turkey and parts of Syria, causing widespread damage and casualties. The first quake, known as the Pazarcık mainshock, had a magnitude of 7.8 and occurred near Gaziantep, about 37 km from the epicentre, at 04:17 TRT (01:17 UTC). The Turkish Accelerometric Database and Analysis System (TADAS), operated by the Disaster and Emergency Management Presidency (AFAD), comprises an extensive ground motion network within the earthquake zone. Data from TADAS indicate that the Pazarcık earthquake resulted in strong ground motions recorded at 380 stations [46, 47]. In this study, records from two of these stations were used in SAP2000 analyses. To improve the quality of the raw data, undesired noise was removed from the recordings. A baseline correction was applied to the horizontal and vertical data to remove long-term drift. A 4th order Butterworth bandpass filter was then used to remove noise frequencies between 0.05 and 25 Hz. Tables 3.1 - 3.3 presents the properties of selected stations, and related GM parameters. These parameters are essential for assessing the seismic risk and designing appropriate earthquake resistant structures in these regions. In addition, Figures 3.2 - 3.3 visualise the time histories and FAS for the corresponding GMs.

The type of a GM can be identified by evaluating the normalized velocity PGV_n as given in Equation 3.2. For instance, a high normalized velocity value (> 0.75) usually indicates a narrow-band GM, denoting a limited frequency range. On the other hand, a low PGV_n value (< 0.45) is indicative of a broad-band GM, suggesting a wide frequency range. There is also an intermediate range, (0.45-0.75), indicating a medium-band GM [48]. In line with this information, the record at Station-3116 is medium-band (PGV_n=0.503), the record at Station-3124 is broad-band GM (PGV_n=0.390), and the record at Station-4613 is broad-band GM (PGV_n=0.334).

$$PGV_n = \frac{PGV}{\sqrt{PGD.PGA}} \tag{3.2}$$

Table 3.1. Properties of the selected stations.

Property	**Station No**		
	3116	**3124**	**4613**
Province	Hatay	Hatay	Kahramanmaraş
District	İskenderun	Antakya	Andırın
Latitude	36.6162	36.2387	37.5701
Longitude	36.2066	36.1722	36.3574
$\boldsymbol{V_{s30}}$ (m/s)	870	283	998
$\boldsymbol{R_{jb}}$ (km)	15.6	0	50.9
$\boldsymbol{R_{epi}}$ (km)	99	13.3	69.5

Table 3.2. Peak ground values.

Station No	**Peak Ground Acceleration (PGA), m/s^2**			**Peak Ground Velocity (PGV), m/s**			**Peak Ground Displacement (PGD), m**		
	EW	NS	UD	EW	NS	UD	EW	NS	UD
3116	1.637	1.577	1.581	0.350	0.380	0.192	0.354	0.482	1.581
3124	6.225	5.747	5.789	0.958	1.112	0.425	0.969	0.456	5.789
4613	1.558	1.459	0.714	0.111	0.138	0.129	0.071	0.093	0.116

Table 3.3. Ground motion parameters.

Ground Motion Parameters	**Station No**					
	3116		**3124**		**4613**	
	EW	**NS**	**EW**	**NS**	**EW**	**NS**
Predominant Period, (s)	0.20	0.14	1.06	0.55	0.09	0.10
Duration D(5-95), (s)	34.30	32.30	18.91	21.87	40.64	41.69
Arias Intensity	0.853	0.793	7.769	6.25	0.629	0.502
Housner Intensity	0.846	0.897	3.914	4.449	0.290	0.276
Cumulative Absolute Velocity, (m/s^2)	12.814	12.982	34.122	32.045	11.897	10.777

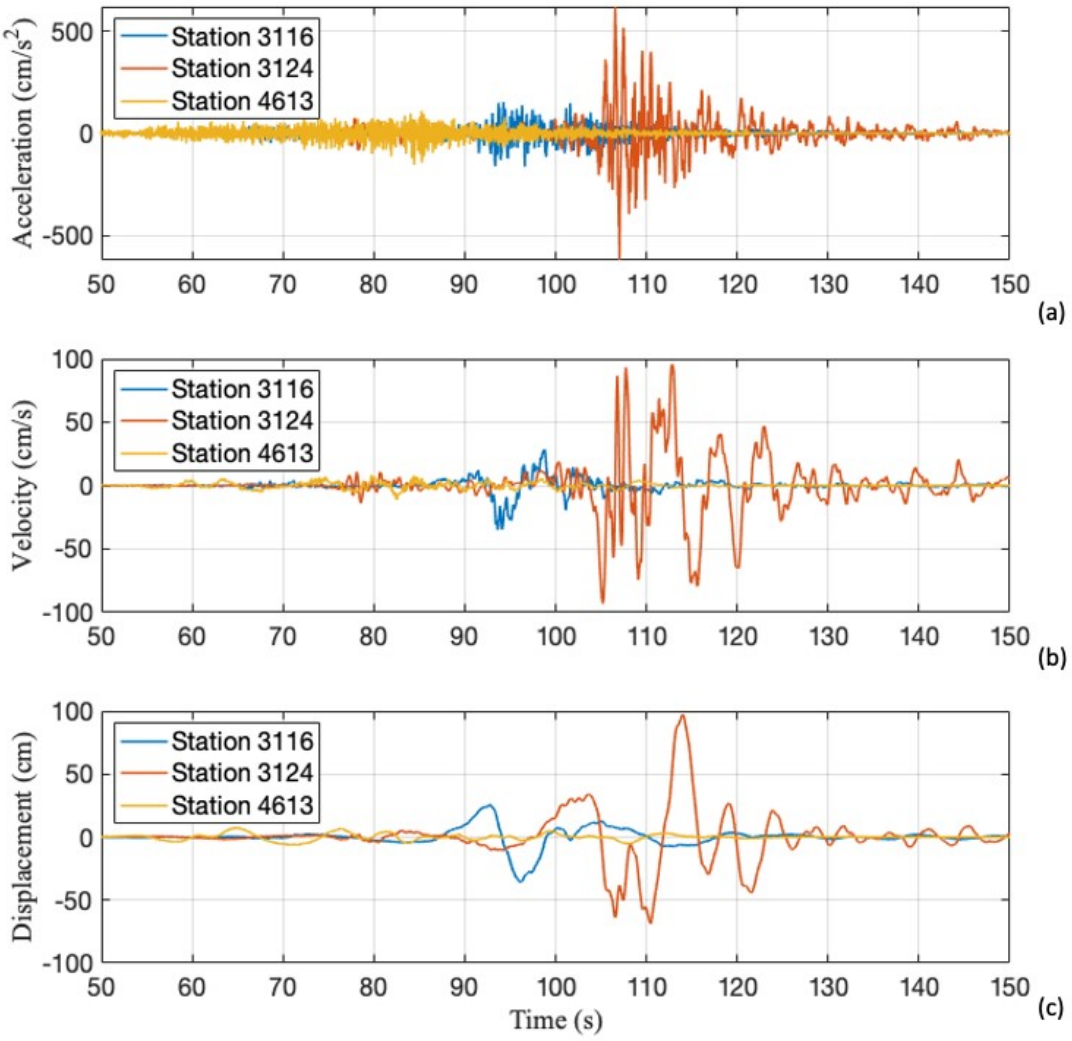

Figure 3.2. EW time histories recorded at the Stations 3116-3124-4613 during the 2023 Kahramanmaraş Earthquake; (a) Ground acceleration, (b) Ground velocity, (c) Ground displacement.

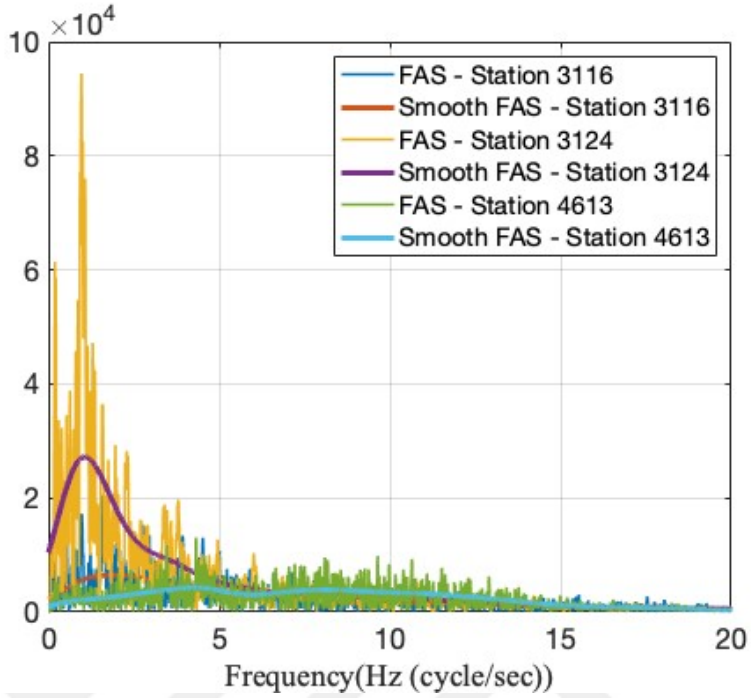

Figure 3.3. Fourier Amplitude Spectrum of EW ground acceleration recorded at the Stations 3116-3124-4613 during the 2023 Kahramanmaraş Earthquake.

3.2. Filter Design in Case Studies

FIFs depend on properties of the foundation system (geometry and embedment depth), direction of the applied load, and the environmet soil. This study adresses two cases (Table 3.4, Figure 3.4) and the properties of soil deposit are given in Table 3.5.

Each case represents a specific type of foundation with varying soil conditions.

Table 3.4. Properties of the considered foundations.

No	Geometry	Embedment	Soil Environment	Movements
FT-1	Circular	Surface	Homogeneous	Horizontal (x)
FT-2	Circular	Surface	Layered on rigid	Horizontal (x)

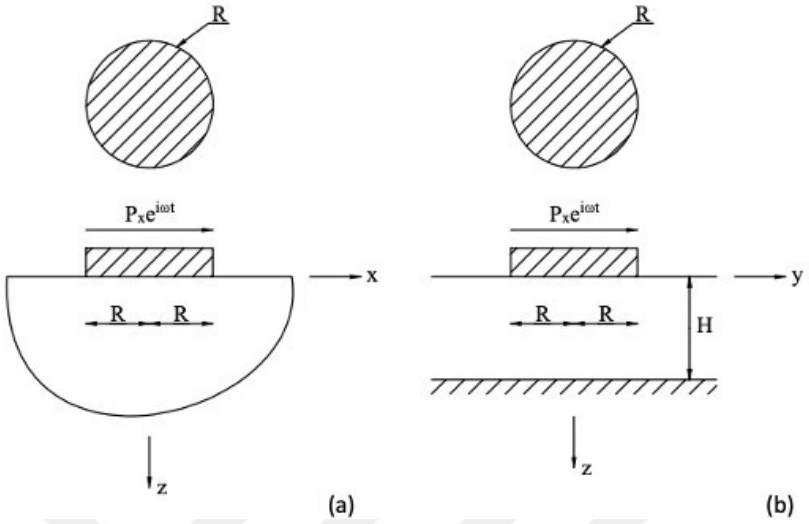

Figure 3.4. Considered foundation types: (a) FT-1, (b) FT-2 (sketches adapted from [44]).

Table 3.5. Properties of the considered soil deposit.

No	**Soil Environment**	**Shear wave velocity (V_s), (m/s)**	**Poisson's ratio (v)**	**Internal (Hysteretic) damping ratio (β)**
FT-1	Homogeneous soil media	400	0.3	0
FT-2	Layered soil media on rigid bedrock	100	0.3	0.05

The calculation of FIF, K(ω), for a foundation surrounded by homogeneous soil media is done using Equation (3.3). However, if the soil media is layered, reflecting the complexity of varying soil properties throughout the soil layers, K(ω) is calculated using Equation (3.4) [44, 49, 50].

$$K(\omega) = K_0[K(a_0) + ia_0C(a_0)] \tag{3.3}$$

$$K(\omega) = K_0[K(a_0) + ia_0C(a_0)](1 + 2i\beta) \tag{3.4}$$

$$a_0 = \frac{\omega R}{V_s} \tag{3.5}$$

where a_0 stands for the dimensionless frequency, and β represents the internal damping ratio. Additionally, ω, R, V_s indicate the angular frequency, the radius of the circular foundation slab, and the shear wave velocity, respectively.

In addition, static stiffness, K_0, is defined by in "Equation (3.6)" for FT-1 [49], and "Equation (3.7)" for FT-2 [50, 51].

$$K_{0(h)} = \frac{8GR}{(2-\nu)} \tag{3.6}$$

$$K_{0(r)} = \frac{8GR}{2-\nu}\left[1+\frac{R}{2H}\right]\left[1+\frac{2D}{3R}\right]\left[1+\frac{5D}{4H}\right] \tag{3.7}$$

$$G = \gamma * (V_s^2) \tag{3.8}$$

where G, ν, γ, H, D, indicate the shear modulus of the soil deposit, Poisson's ratio, the unit weight of the soil, the thickness of the layered soil media, and the depth of foundation, respectively.

Figure 3.5(b) examines the interrelation between the dimensionless frequency and the FIF parameters related to FT-1, which is a circular foundation (R=10m) located on the ground surface and exposured to horizontal movement. The stiffness coefficient decreases as the dimensionless frequency increases, indicating increased flexibility. Additionally, the damping coefficient generally increases, implying improved energy absorption capabilities. A zero mean Gaussian function, Figure 3.5(c), with a standard deviation of 15 is employed in this case. Optimal filter orders were determined by measuring the decrease in filter error as m increased, and the filter order was chosen as m=2 and n=1. The filter parameters were determined through the use of the least-squares method, which incorporates the Gaussian weighting function to improve accuracy: $a_0 = 1.0000$, $a_1 = 1.0422$, $a_2 = 0.1056$, $b_0 = 4.1540$, and $b_1 = -2.0235$ (Table 3.6). The filter stability is given in Figure 3.5(d). The calculated time-domain amplitudes and phases are compared with the frequency-domain results in Figure 3.5(e) and Figure 3.5(f).

Figure 3.6 shows the results for FT-2, which is the circular (R=10m) surface foundation surrounded by layered soil media (H=2R) on rigid bedrock, and it is exposed to horizontal movement. When examining the components of the FIF of FT-2, in Figure 3.6(b), it is observed that as the dimensionless frequency increases, the stiffness experiences a decrease with a fluctuating downward trend, whereas the damping shows the opposite effect with a fluctuating upward trend. While option (c) and (d) present that the related Gaussian weighting function and the filter stability check, option (e) and (f) indicate that frequency and time-domain filters overlap well with each other due to the selected parameters.

The following figures demonstrates the analysis of two diverse footing types, and the accompanying tables contain the filter parameters that were determined in the time-domain filter's design.

$$y(t) = -1.0422y(t-1)-0.1056y(t-2)+K_0[4.1540x(t)-2.0235x(t-1)] \quad (3.9)$$

$$H(\omega) = K_0\frac{4.1540 - 2.0235z^{-1}}{1 + 0422z^{-1} + 0.1056z^{-2}} \quad (3.10)$$

Table 3.6. Standard deviation, filter orders and filter parameters for FT-1.

Footing Type	**Standard Deviation**	**Filter Orders**		**Filter Coefficients**		R^2	
		m	**n**	**a**	**b**	**Mag**	**Phase**
FT-1	15	2	1	a0=1.0000 a1=1.0422 a2=0.1056	b0=4.1540 b1=-2.0235	0.9991	0.9998

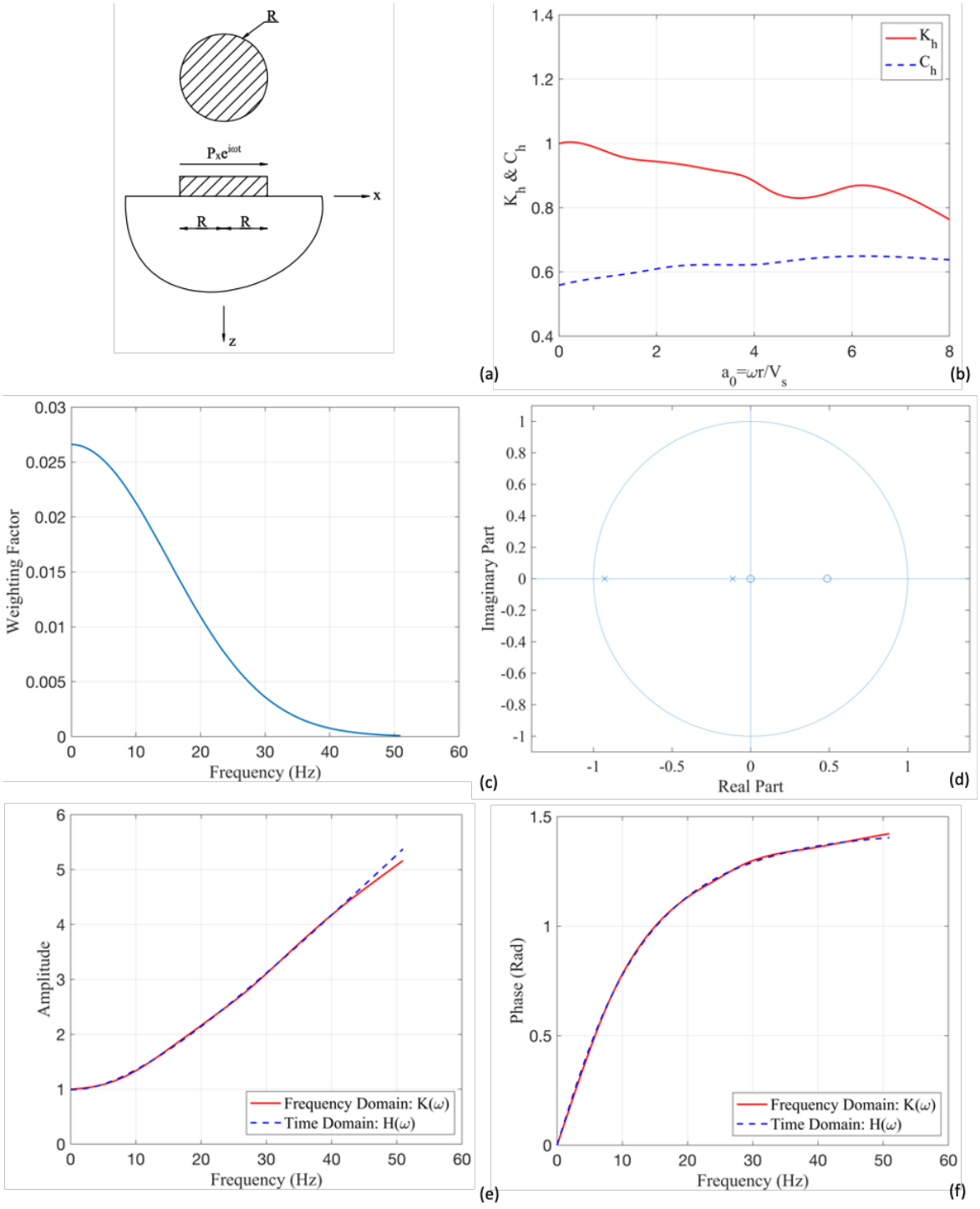

Figure 3.5. (a) Sketch of FT-1, (b) The components of FIF: stiffness and damping, (c) the Gaussian weighting function, (d) the filter stability by z-plane, (e) comparison of frequency and time domain IFs in terms of amplitudes, (f) comparison of frequency and time domain IFs in terms of phases for the case FT-1.

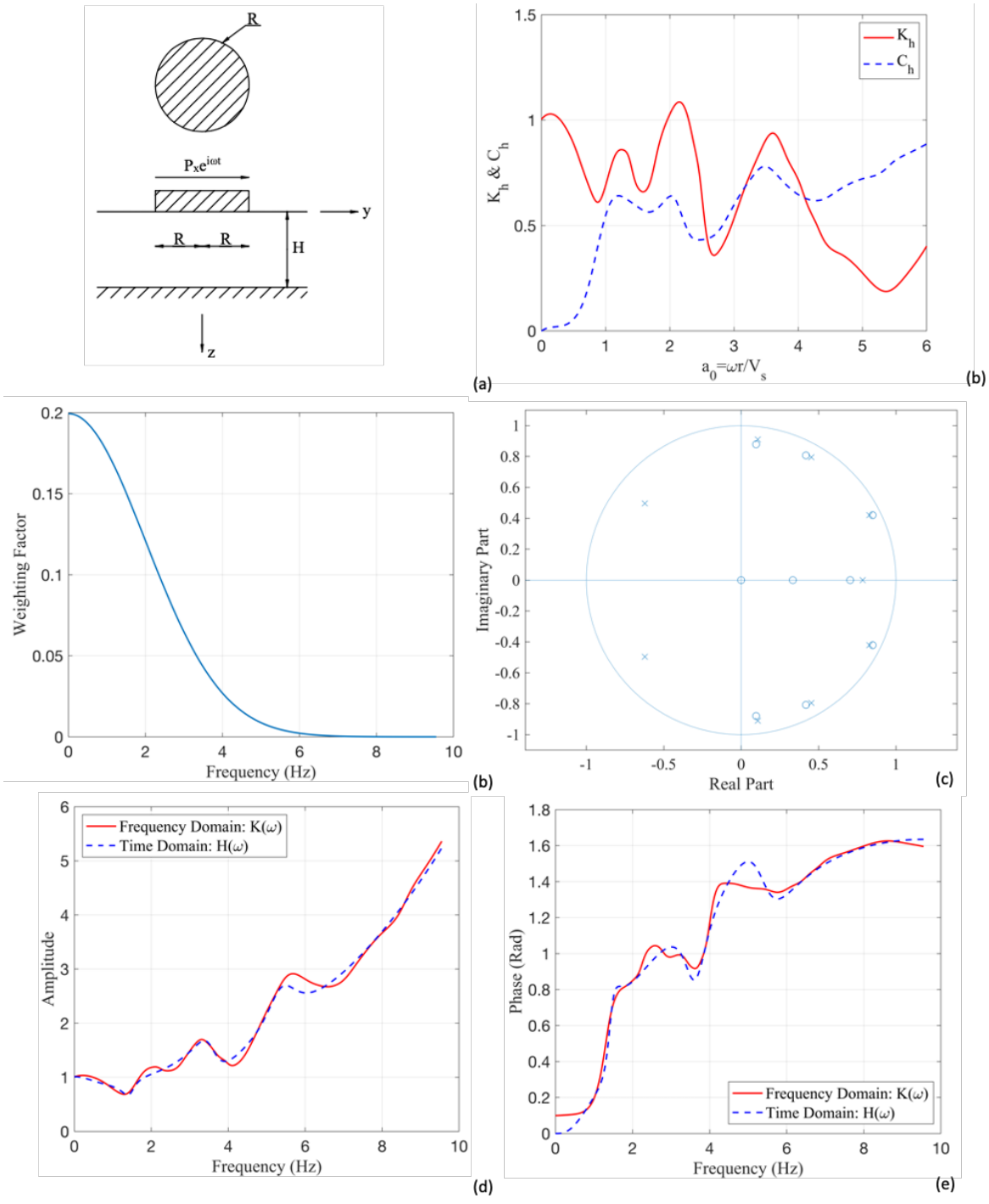

Figure 3.6. (a) Sketch of FT-2, (b) The components of FIF: stiffness and damping, (c) the Gaussian weighting function, (d) the filter stability by z-plane, (e) comparison of frequency and time domain IFs in terms of amplitudes, (f) comparison of frequency and time domain IFs in terms of phases for the case FT-2.

Table 3.7. Standard deviation, filter orders and filter parameters for FT-2.

Footing Type	**Standard Deviation**	**Filter Orders**		**Filter Coefficients**		**R^2**	
		m	**n**	**a**	**b**	**Mag**	**Phase**
FT-2	2	9	8	a0=1.0000 a1=-2.3189 a2=2.9748 a3=-2.4449 a4=1.3808 a5=-0.7579 a6=0.8564 a7=-0.9689 a8=0.7739 a9=-0.3014	b0=3.1703 b1=-11.9420 b2=23.7326 b3=-31.6191 b4=30.3824 b5=-21.2429 b6=10.5558 b7=-3.2734 b8=0.4325	0.9939	0.9910

3.3. Applications of Time Domain Filters in Case Studies

Figure 3.7 and Figure 3.8 compare the FFMs with those that have undergone different impedance functions. The varied FIMs were obtained from ground motion with low-frequency content (RW1 in Figure 3.7), and high-frequency content (RW2 in Figure 3.8).

Figure 3.7 illustrates that the maximum acceleration recorded for the FIM with FT-1 is 1.0078 m/s^2 at around 5.02 seconds. The three curves representing FFM (RW1), FIM (FT-1), and FIM (FT-2) exhibit a similar trend, with each reaching its peak near the 5-second mark. The proximity of these curves indicates a slight variation between the filter methods. The results indicate that circular surface foundations exhibit similar behavior under this input motion in different soil environments, whether homogeneous or layered on rigid soil.

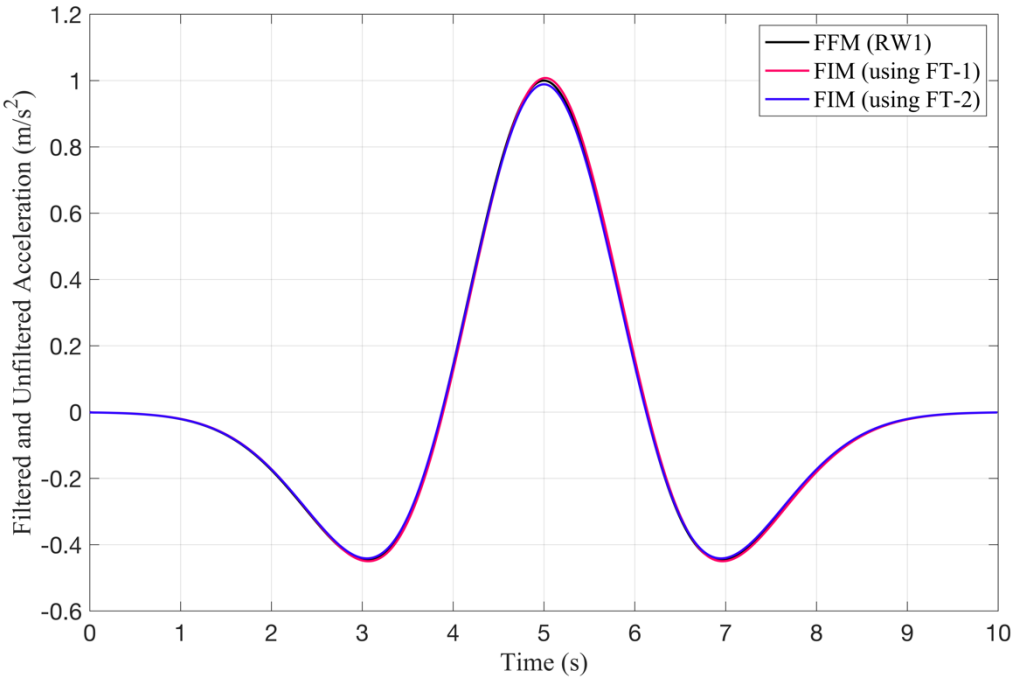

Figure 3.7. Comparison of the filtered and unfiltered acceleration, under RW1.

Figure 3.8 (FIM using RW2) shows a similar trend of increasing acceleration, with a peak of 0.9662 m/s² at approximately 0.41 seconds for FIM with FT-1. This suggests that there is some attenuation in the acceleration that reaches the structure, which is desirable for reducing seismic forces. In contrast, FIM with FT-2 exhibits a slightly higher peak of 1.0793 m/s², occurring marginally earlier at 0.4 seconds. This graph highlights the variation between the two filtering methods, suggesting that FT-2 may be more responsive to acceleration changes than FT-1.

When comparing the two graphs (in Table 3.8) and their respective peak accelerations, it is observed that FIM using FT-2 in RW2 had the highest peak acceleration of all the trials, although it occurred earlier than the peak in RW1. The time to reach peak acceleration is noticeably different between RW1 and RW2, indicating a possible variation in the dynamics of the two events.

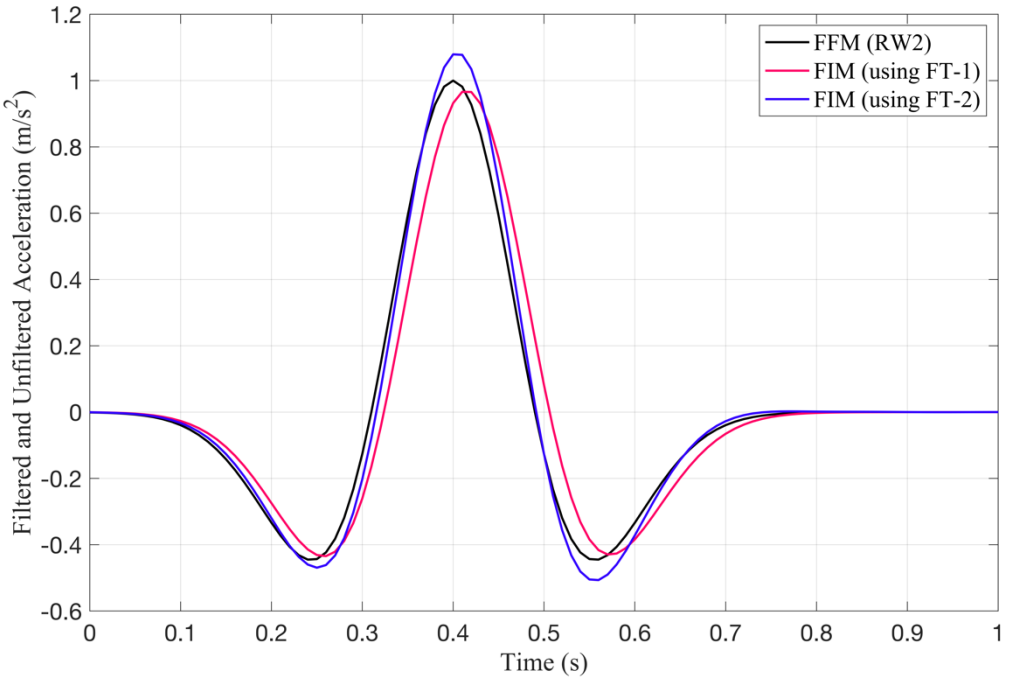

Figure 3.8. Comparison of the filtered and unfiltered acceleration, under RW2.

Table 3.8. Peak acceleration and its time (considering Ricker wavelet).

Input		**FFM**	**FIM/FT-1**	**FIM/FT-2**
RW1	**Peak Acceleration** (m/s^2)	1	1.0078	0.9888
	Time (s)	5	5.02	5
RW2	**Peak Acceleration** (m/s^2)	1	0.9662	1.0793
	Time (s)	0.4	0.41	0.4

Figures 3.9 - 3.11 show a comparison of FFM and FIM accelerations and Fourier amplitude spectrum during the 2023 Kahramanmaraş Earthquake recorded at stations 3116, 3124 and 4613. The Table 3.9 related to the figures show that FIM/FT-2 has higher peak acceleration amplitudes than both FFM and FIM/FT-1. This suggests that structures built on foundation type 2 are subject to greater acceleration increases.

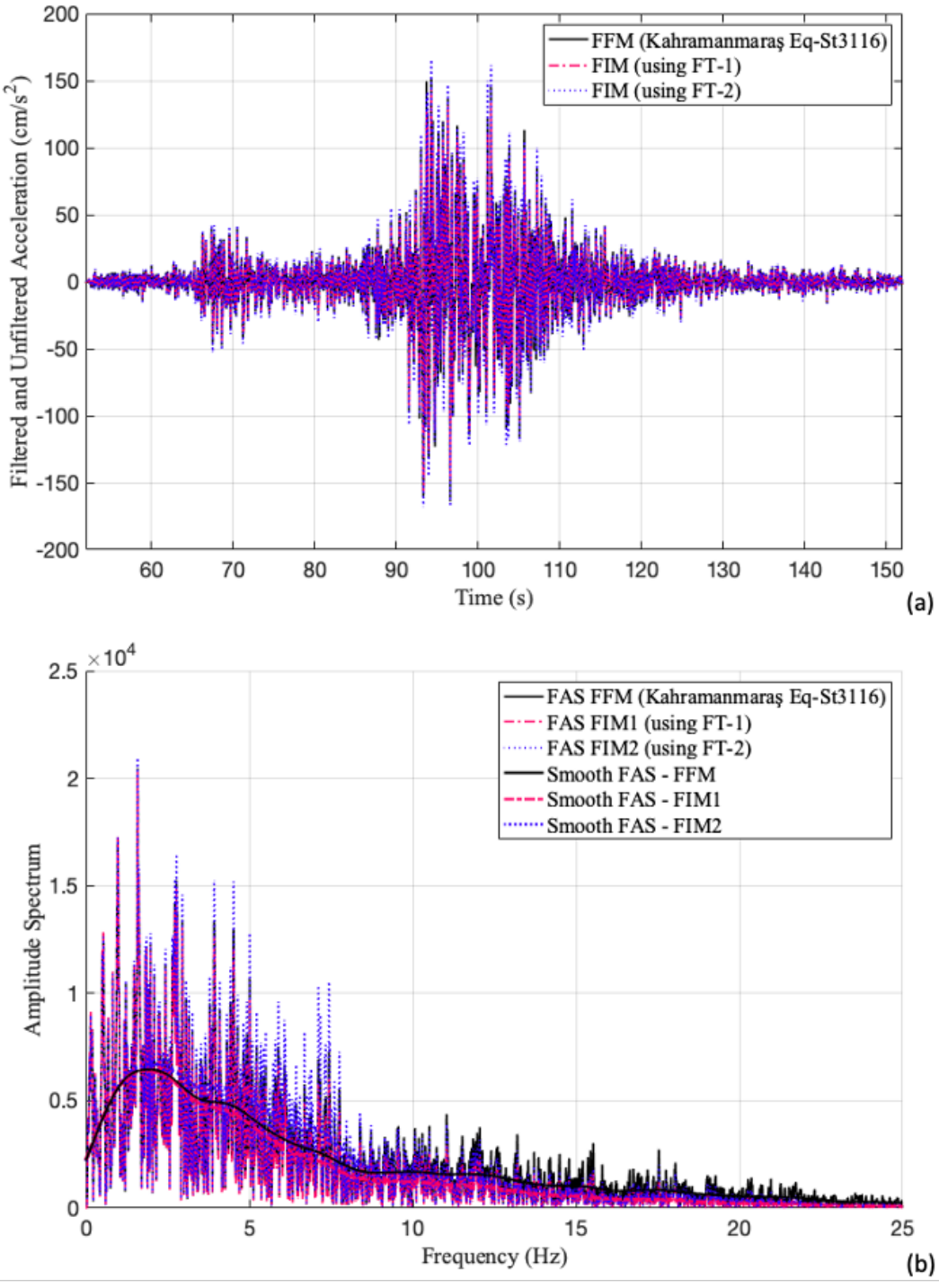

Figure 3.9. Comparison of the filtered and unfiltered (a) acceleration, and (b) FAS, under the EW ground acceleration recorded at the Station-3116 during the 2023 Kahramanmaraş Earthquake.

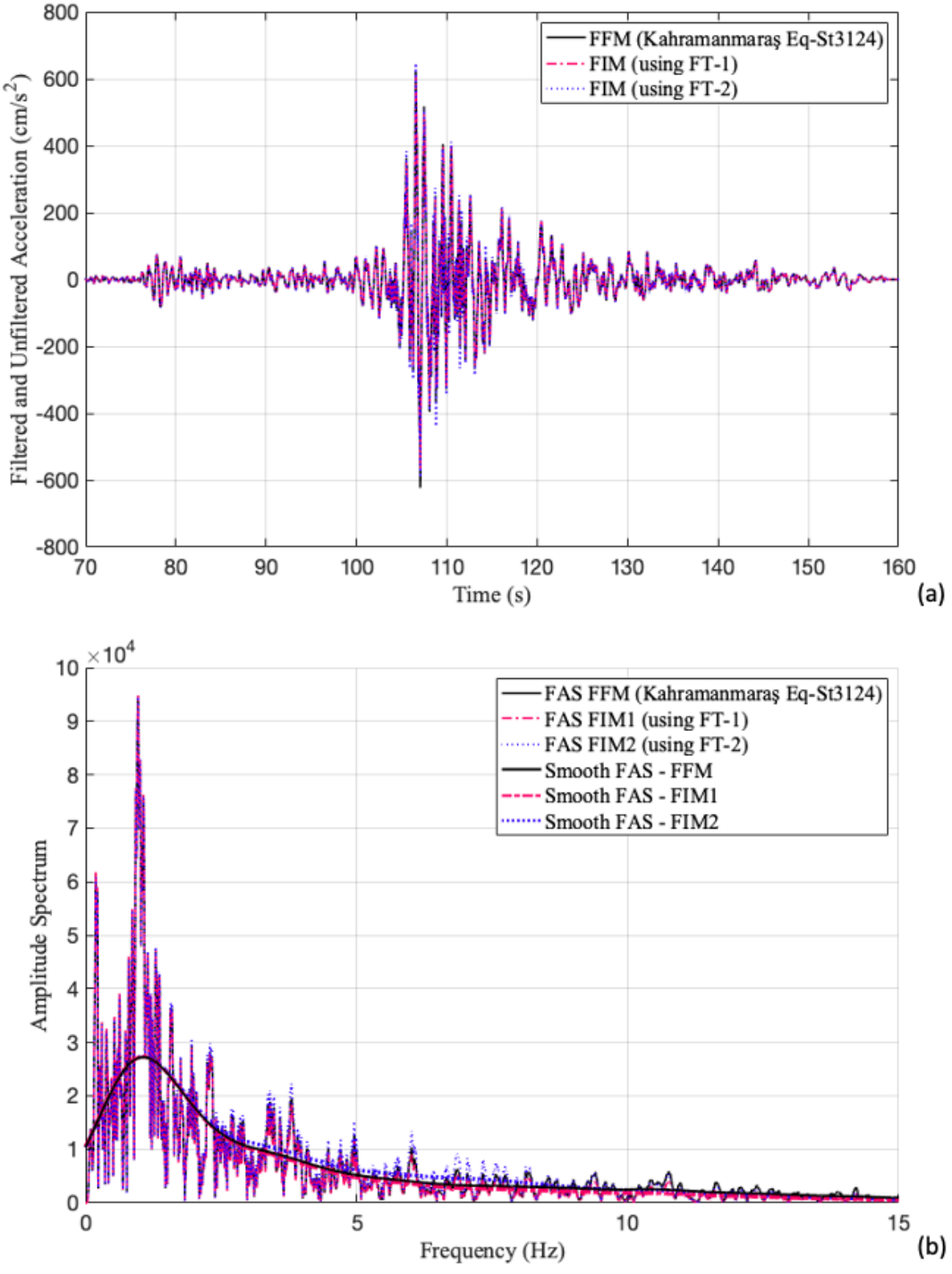

Figure 3.10. Comparison of the filtered and unfiltered (a) acceleration, and (b) FAS, under the EW ground acceleration recorded at the Station-3124 during the 2023 Kahramanmaraş Earthquake.

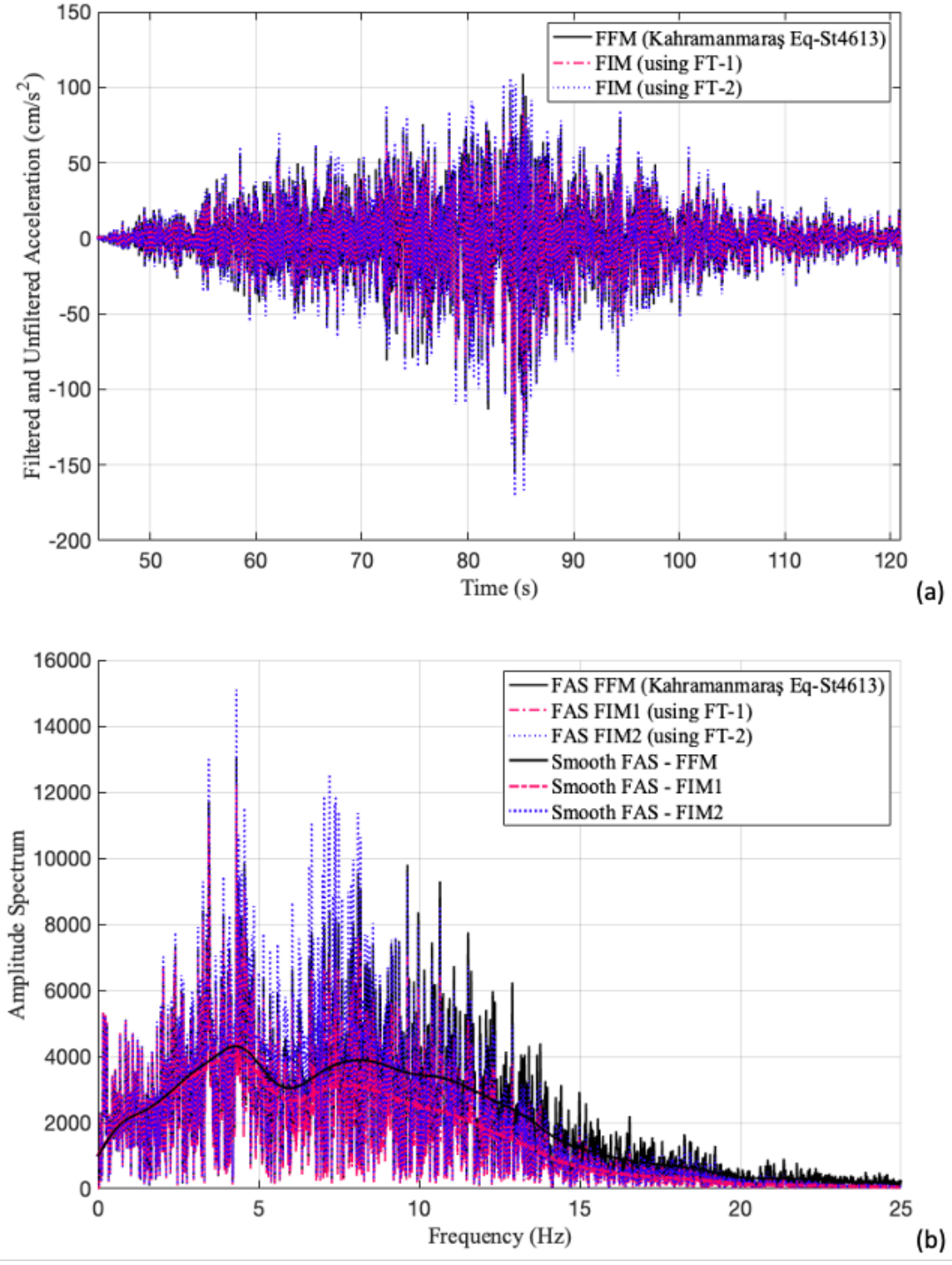

Figure 3.11. Comparison of the filtered and unfiltered (a) acceleration, and (b) FAS, under the EW ground acceleration recorded at the Station-4613 during the 2023 Kahramanmaraş Earthquake.

Table 3.9. Peak acceleration and its time (considering Kahramanmaraş Earthquake).

Input		**FFM**	**FIM/FT-1**	**FIM/FT-2**
Station-3116	**Peak Acceleration** (m/s^2)	163.7254	157.8378	168.2918
	Time (s)	96.62	93.35	93.34
Station-3124	**Peak Acceleration** (m/s^2)	622.485	608.9732	646.049
	Time (s)	107.04	106.57	106.56
Station-4613	**Peak Acceleration** (m/s^2)	155.7579	131.2301	170.7083
	Time (s)	84.44	84.45	84.45

3.4. SSI Effects on Response Spectra

Understanding the relationship between SSI and seismic response is crucial in earthquake engineering. SSI is composed of two parts: kinematic effects and inertial effects. Since we are only interested in the effects of foundation geometry and assume a massless foundation, we are considering only the kinematics part of SSI. This interplay can greatly affect the dynamic behavior of structures during seismic events. In this study, the elastic dynamic response of idealized systems (SDOF) was determined using the Newmark Linear Method [52].

To calculate the dynamic response of a structure, the earthquake load represented by FIM data (updated FFM), is integrated into the analytical framework. The parameters required for implementing the Newmark Linear Method, namely the acceleration factor ($\beta = 1/4$) and the velocity factor ($\gamma = 1/2$), are then specified using the average acceleration method due to its balance of stability and accuracy. This is a typical de-

fault choice in many structural dynamics applications unless there is a specific reason to choose a less accurate or more conditionally stable method. The structural state variables (displacement, velocity, and acceleration) are initialized to zero to serve as the initial conditions. The Newmark Linear Method is then used iteratively to compute the translational response to seismic excitation.

The acceleration at each time step is determined by resolving the linear equations formulated using the Newmark Linear Method. The displacement (Equation 3.11) and velocity (Equation 3.12) are then updated iteratively based on the newly calculated acceleration, enabling a time-stepped simulation of the response to seismic forces.

$$d(ti) = d(i-1) + \nu(i-1)\Delta t + ((1-2\beta)a(i-1) + 2\beta a(i))\frac{\Delta t^2}{2} \quad (3.11)$$

$$\nu(i) = \nu(i-1) + ((1-\gamma)a(i-1) + \gamma(i))\Delta t \quad (3.12)$$

Figure 3.12 represents the illustrations of translational response spectra with Ricker wavelet (RW1 and RW2) charting spectral acceleration versus vibration period for three different motions: Free Field Motion (FFM), Foundation Input Motion using footing type 1 (FIM-1), and type 2 (FIM-2). Figure 3.12(a) shows that RW1, with a resonance frequency of 0.2 Hz, has overlapping spectral accelerations for FFM, FIM-1, and FIM-2, indicating that the type of footing has little impact on the response in this frequency range. In Figure 3.12(b), representing RW2 with a resonance frequency of 2.5 Hz, there is a noticeable divergence in peak PSA values for FIM-1 and FIM-2 from FFM, indicating a more significant effect of footing type at higher frequencies.

Investigating the seismic response of various foundation types under different frequency content of ground motion provides valuable insights into foundation behavior. The response spectra, derived from Ricker-type pulses with distinct resonance frequencies, offer a comparative framework for analyzing the influence of footing design on seismic input motions. With RW1's resonance at 0.2 Hz, the spectra for FFM, FIM-1, and FIM-2 are closely aligned, indicating a minimal impact of foundation type in lower frequency ranges. This suggests that the dynamic characteristics of the foundation

are less sensitive to the footing configuration under long-period ground motions. Conversely, at a higher resonance frequency of 2.5 Hz for RW2, the FFM curve is notably separated from FIM-1 and FIM-2, particularly at shorter periods. This highlights that the FT can amplify dynamics at higher frequencies. The peak spectral acceleration for FIM-1 exceeds that of FFM, due to the foundation's impedance effects, which could increase the demands on structural elements during seismic events.

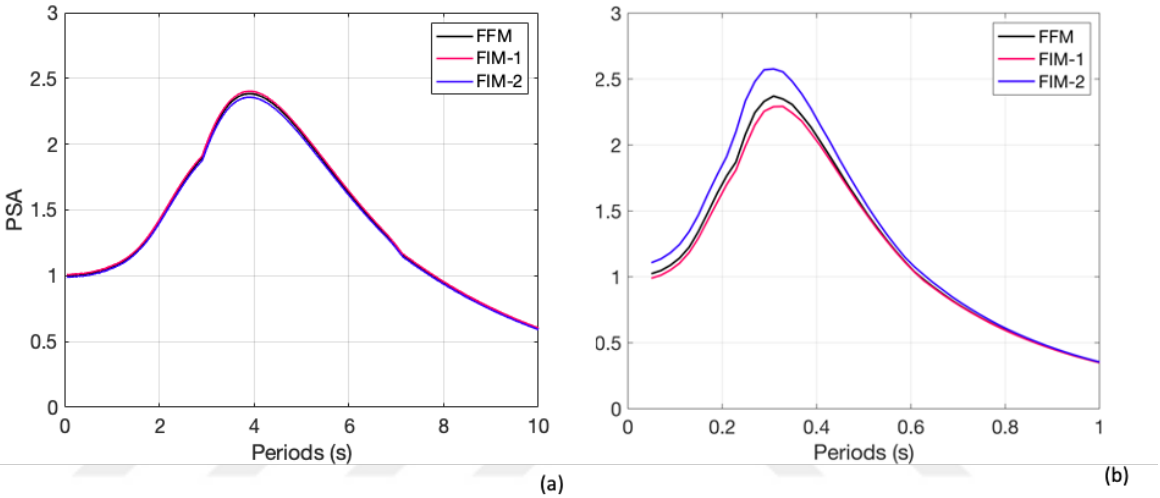

Figure 3.12. Translational response considering (a) RW1, and (b) RW2.

The Tables 3.10 and 3.11 display SA values at different periods for FFM, FIM-1, and FIM-2 under two distinct simulated seismic records, RW1 and RW2, respectively. SA is a critical parameter for seismic design and evaluation of structures to resist seismic forces as it quantifies the peak acceleration that a structure is expected to experience at specific vibration periods. The table shows that for RW1, the T_1 is consistently 3.91 seconds for all ground motions, including FFM, FIM-1, and FIM-2. The SA at the T_1 is similar across all input motions. When considering a period that is 1.5 times longer than the T_1, the SAs are shown to exhibit a slight decrease for all inputs. This trend is typical due to the decrease in responsiveness of structures at periods longer than their natural period. The SA across the range from $0.2T_1$ to $1.5T_1$ is relatively uniform among the cases, with minimal variance. For the second seismic event, RW2, the T_1 of the ground motions are significantly shorter. This suggests either a different structural dynamic or a change in the frequency content of the seismic event. At these shorter fundamental periods, the recorded SA values differ slightly from RW1.

At 1.5 times the fundamental period, the SAs for RW2 are lower than those at T_1, as observed in RW1. This conforms to the expected decrease in structural response beyond the fundamental period. Finally, the average spectral acceleration for RW2 is in the range of $0.2T_1$ to $1.5T_1$ is highest for FIM-2 at 1.98 m/s^2. Considering RW2, FIM-2 may be the most demanding in terms of spectral response, requiring resilient design considerations. These comparisons are important for evaluating earthquake engineering designs to ensure that structures can withstand seismic events. The consistent T_1 under RW1 and its significant decrease under RW2 may indicate changes in seismic energy or variations in the dynamic properties of the analyzed structural models.

Table 3.10. The SA values at different periods are provided for FFM as RW1.

Ground Motion	**FFM**	**FIM-1**	**FIM-2**
$\boldsymbol{T_1, (s)}$	3.91	3.91	3.91
$\boldsymbol{S_a(T_1), (m/s^2)}$	2.38	2.40	2.36
$\boldsymbol{S_a(1.5T_1), (m/s^2)}$	1.69	1.70	1.67
$\boldsymbol{AvgS_a(0.2T_1 - 1.5T_1), (m/s^2)}$	1.83	1.84	1.81

Table 3.11. The SA values at different periods are provided for FFM as RW2.

Ground Motion	**FFM**	**FIM-1**	**FIM-2**
$\boldsymbol{T_1, (s)}$	0.31	0.33	0.31
$\boldsymbol{S_a(T_1), (m/s^2)}$	2.37	2.29	2.58
$\boldsymbol{S_a(1.5T_1), (m/s^2)}$	1.72	1.54	1.80
$\boldsymbol{AvgS_a(0.2T_1 - 1.5T_1), (m/s^2)}$	1.82	1.75	1.98

Figures 3.13 - 3.15 illustrate the translational response spectra of real earthquakes recorded at the three stations (Stations 3116-3124-4613) during the 6 February 2023 Kahramanmaraş Earthquake. The figures chart the spectral acceleration versus period for three different input motions: FFM, FIM-1, and FIM-2. The following Tables 3.1 2- 3.14 show the SA values at different periods for FFM, FIM-1, and FIM-2, based on three real earthquake records.

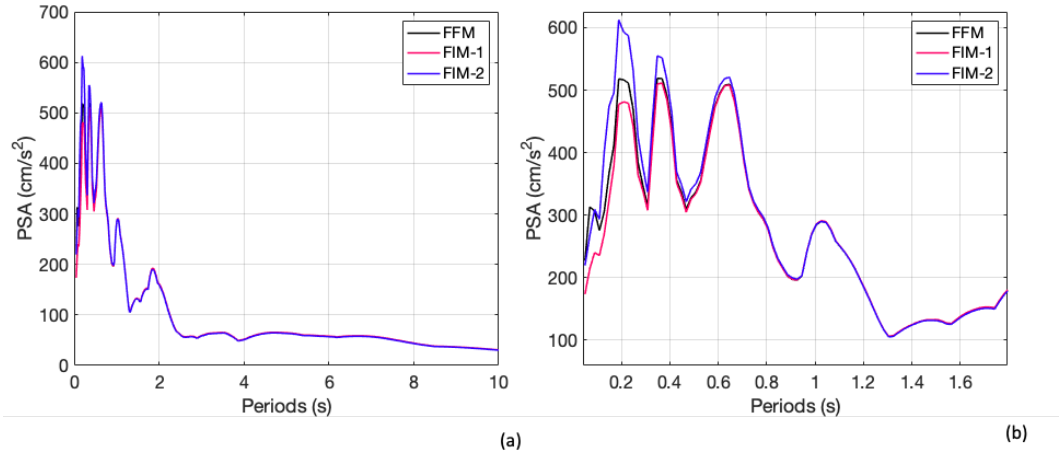

Figure 3.13. Translational response considering the EW ground acceleration recorded at Station-3116 during the 2023 Kahramanmaraş Earthquake (a) full view, and (b) zoom view in shorter periods.

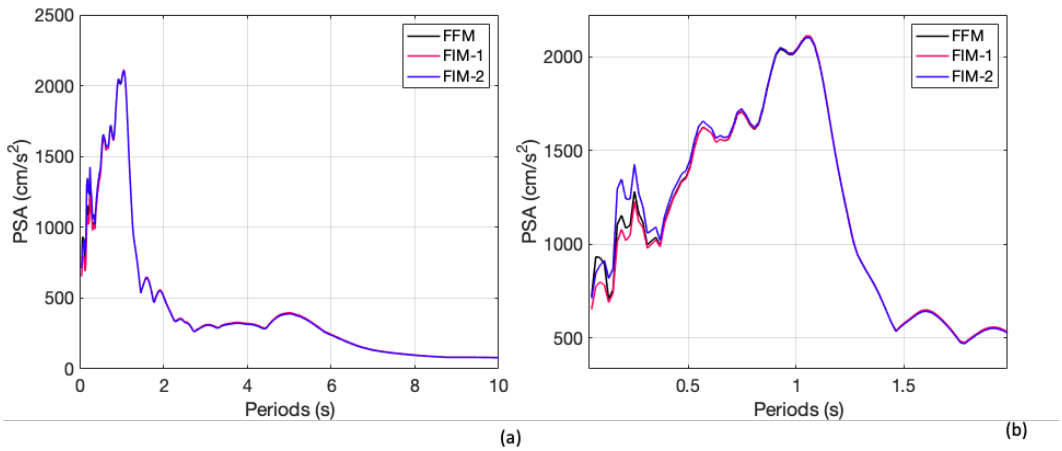

Figure 3.14. Translational response considering the EW ground acceleration recorded at Station-3124 during the 2023 Kahramanmaraş Earthquake (a) full view, and (b) zoom view in shorter periods.

At Station-3116, the SA values at T_1 indicate that FIM-2 displays the highest SA with a value of 612.6535 cm/s^2. FFM and FIM-1 follow with slightly less values at 519.0554 cm/s^2 and 511.4361 cm/s^2, respectively. At $1.5T_1$, FIM-1 exhibits the highest SA value, with a value of 404.0518 cm/s^2. However, FIM-2 demonstrates the highest average SA across the $0.2T_1 - 1.5T_1$ range, indicating a superior dynamic response for this footing type at this location.

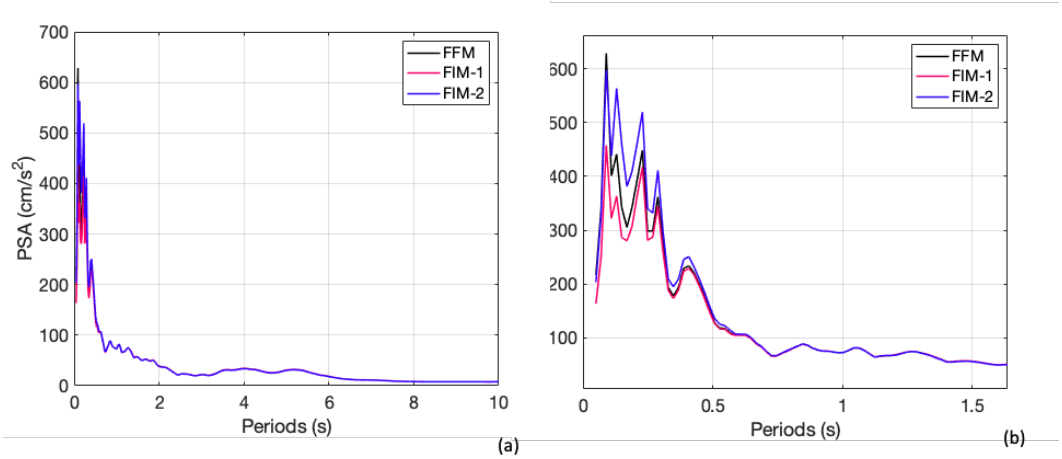

Figure 3.15. Translational response considering the EW ground acceleration recorded at Station-4613 during the 2023 Kahramanmaraş Earthquake (a) full view, and (b) zoom view in shorter periods.

Table 3.12. The SA values at different periods are provided for FFM considering Kahramanmaraş Earthquake (Station-3116).

Ground Motion	**FFM**	**FIM-1**	**FIM-2**
$\boldsymbol{T_1, (s)}$	0.3485	0.3684	0.1893
$\boldsymbol{S_a(T_1), (m/s^2)}$	519.0554	511.4361	612.6535
$\boldsymbol{S_a(1.5T_1), (m/s^2)}$	350.6970	404.0518	389.3224
$\boldsymbol{AvgS_a(0.2T_1 - 1.5T_1), (m/s^2)}$	395.8716	378.7016	434.3714

Table 3.13. The SA values at different periods are provided for FFM considering Kahramanmaraş Earthquake (Station-3124).

Ground Motion	**FFM**	**FIM-1**	**FIM-2**
$\boldsymbol{T_1, (s)}$	1.0450	1.0450	1.0450
$\boldsymbol{S_a(T_1), (m/s^2)}$	2102.4328	2111.3869	2104.58
$\boldsymbol{S_a(1.5T_1), (m/s^2)}$	633.1401	637.0442	630.0301
$\boldsymbol{AvgS_a(0.2T_1 - 1.5T_1), (m/s^2)}$	1365.5303	1363.8892	1386.4552

At Station-3124, the SA values for all input motions remain relatively stable at T_1. In particular, FFM is at 2102.4328 cm/s^2, FIM-1 at 2111.3869 cm/s^2, and FIM-2 at 2104.58 cm/s^2. Similarly, at $1.5T_1$, the SA values exhibit minor fluctuations but remain consistent. The dynamic responses of all the input motions at this station are consistent, as indicated by the comparable average SA between $0.2T_1$ and $1.5T_1$.

Table 3.14. The SA values at different periods are provided for FFM considering Kahramanmaraş Earthquake (Station-4613).

Ground Motion	**FFM**	**FIM-1**	**FIM-2**
$\boldsymbol{T_1, (s)}$	0.0898	0.0898	0.0898
$\boldsymbol{S_a(T_1), (m/s^2)}$	628.3985	457.4077	597.201
$\boldsymbol{S_a(1.5T_1), (m/s^2)}$	415.6904	343.7324	536.6391
$\boldsymbol{AvgS_a(0.2T_1 - 1.5T_1), (m/s^2)}$	405.126	311.3966	425.8893

The SA values at period T_1 for Station-4613 indicate that the FFM has the highest acceleration at 628.3985 cm/s^2. This is followed by the FIM-2 and FIM-1, with accelerations of 597.201 cm/s^2 and 457.4077 cm/s^2, respectively. However, at $1.5T_1$, the FIM-2 exhibits the highest SA value of 536.6391 cm/s^2, surpassing the others. Furthermore, when considering the average SA over the range $0.2T_1$ to $1.5T_1$, the FIM-2 once again emerges as the most responsive. This indicates that the FIM-2 may demonstrate a greater dynamic response at this specific station.

The comparative analysis of SA values at different periods shows the pivotal importance of FT selection in seismic design. This is because the selection of a foundation model significantly impacts the dynamic response of structures at various stations. Station-3116 exhibits the greatest variation in these values, with the FIM-2 typically producing higher results. In contrast, Station-3124 demonstrates consistent values across all inputs, indicating a uniform dynamic response. Notable discrepancies in SA values at Station-4613, particularly for FIM-2, highlight the necessity for careful foundation model selection.

These findings highlight the significance of taking into account the foundation type in seismic design, especially for structures that are expected to encounter high-frequency ground motions. Additionally, the comparative analysis of FIM-1 and FIM-2 indicates that the specific design details of the footing can also alter the input motion, potentially impacting the seismic performance of the superstructure. The detailed analysis of response spectra is crucial for seismic design engineers to guarantee the safety and performance of structures during earthquakes, considering the effects of kinematic SSI.

3.5. Kinematic SSI Effects on a Five-Story Building: Linear Analysis under 2023 Kahramanmaraş Earthquake Records

This research used data from the 2023 Kahramanmaraş Earthquake collected from three stations (Stations 3116, 3124 and 4613) to analyse the effects of kinematic soil-structure interactions using the SAP2000 structural analysis and design program. Two types of foundation input motions and free field motions were compared across all stations and a five-story model of a symmetrical building was evaluated. A previous study informed the design of the building model, the structural period of which is 0.61sec used in this section [53], and the corresponding visualisation is shown in Figure 3.16. Critical seismic design parameters, i.e. story displacements, story drifts, story and base shear forces, were compared in linear analyses. These parameters measure the safety of a structure by measuring the displacement of the floor relative to the ground, the difference in horizontal displacement between successive floors, and the total horizontal force transmitted from the structure to its foundation (Figures 3.18 - 3.23).

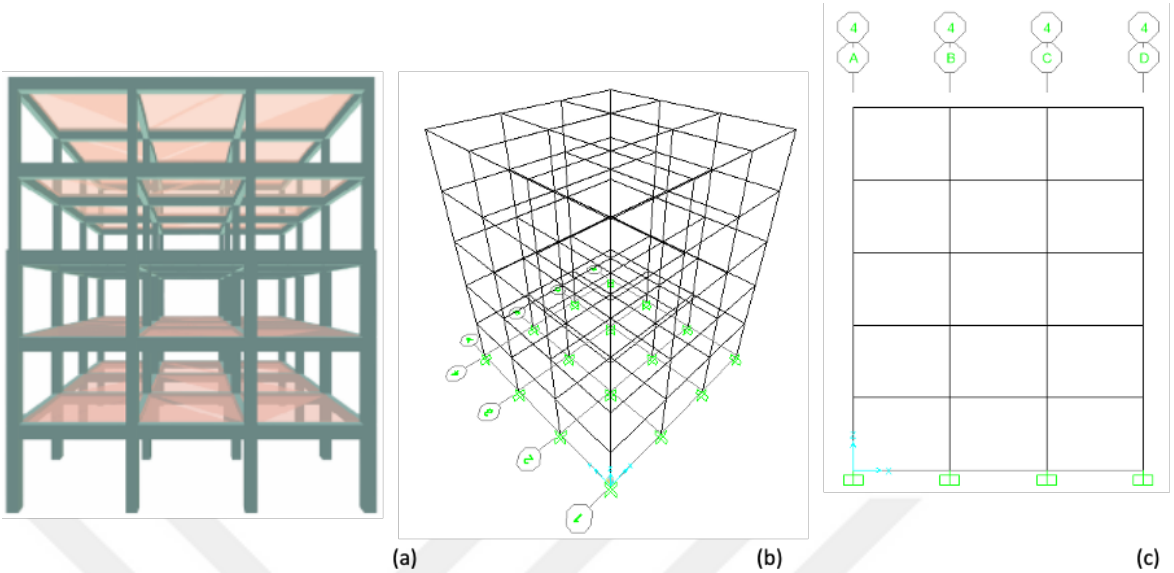

Figure 3.16. Structural model; (a) 3D model (ideCAD), (b) 3D model (SAP2000), (c) X-Z plane (SAP2000) [53].

Figures 3.17 to 3.20 present a linear analysis results of each scenario, detailing the story displacement and drift values. Figure 3.17 and 3.19 demonstrate variations in story displacement and drift across different stations, with a limited x-axis scale to focus on significant differences related to FFM. Subsequently, Figure 3.18 and 3.20 show the full range of story displacement and drift values for a comprehensive comparison of different foundation input motions (FFM, FIM-1, FIM-2), respectively. A review of these results leads to several critical observations:

(i) Station-3116: The results indicate that the differences between FFM, FIM-1, and FIM-2 are minimal, suggesting that considering foundation types yields similar displacement distributions for this station. FIM-2 tends to exhibit slightly higher displacements, while FIM-1 has slightly lower values than FFM.

The top displacement values under FFM, FIM-1, and FIM-2 were found to be 6.43 cm, 6.24 cm, and 6.58 cm, respectively. The top displacement under FIM-1 is slightly lower than under FFM, with a numerical difference of -0.19 cm, representing a decrease of 2.95%. Conversely, the displacement under FIM-2 is

found to exceed that of FFM by an increase of 0.34 cm, representing a 5.45% rise.

The phenomenon of story drift, which refers to the shifting between two adjacent levels of a building, is a crucial element in the assessment of seismic resilience in structures.

The story drifts observed for Station-3116:
FIM-1: There is a general reduction in story drifts in comparison to FFM, with percentage reductions ranging from 1.10% to 5.61%.
FIM-2: Story drifts exhibit a slight increase compared to FFM, with percentage increases ranging from 0.85% to 5.45%. These variations suggest that FIM-1 has a slight mitigating effect on story drifts, while FIM-2 tends to slightly amplify them.

(ii) Station-3124: The results demonstrate elevated displacements, particularly in the upper floors under FFM in this station. The displacement and drift values are also influenced by the foundation modifications. Similar to Station-3116, the differences are noticeable but not substantial. The FIM-1 results are slightly lower overall, while the FIM-2 results tend to be slightly higher and very close to FFM. These differences are due to the high PGA and broadband nature of the ground motions recorded at this particular station.

The top displacement values were observed to be 12.66 cm (FFM), 11.67 cm (FIM-1), and 12.76 cm (FIM-2). The displacement under FIM-1 exhibited a reduction of 0.99 cm in comparison to FFM, indicating a decrease of 7.82%. However, the displacement under FIM-2 is slightly higher than that of FFM, by 1.09 cm, which corresponds to an increase of 9.34%.

(iii) Station-4613: The station records consistently low displacement and drift values. This station shows more significant differences between the FFM, FIM-1, and FIM-2. The FFM provides the lowest displacement values, while the FIM-1

shows the highest at lower stories, and the FIM-2 generally falls in between. This indicates a potential sensitivity to the foundation type at this station. This may be attributed to the wide range of ground motions recorded and a comparatively high V_{s30}, which has resulted in reduced displacement requirements.

The top displacement values observed under the three input motions were considerably lower than those at the other stations, with values of 0.54 cm (FFM), 0.44 cm (FIM-1), and 0.57 cm (FIM-2). Under FIM-1, the displacement was reduced by 0.10 cm, which is equivalent to a decrease of 18.52%. In comparison to FFM, there was an increase of 0.13 cm under FIM-2, representing a 29.55% rise.

The story drifts observed for Station-4613:
FIM-1: There were notable alterations in the data, with the initial story drift increasing by 125%. However, subsequent stories exhibited both positive and negative fluctuations, ranging from a decrease of 10% to an increase of 58.82%.
FIM-2: The results were heterogeneous, with increases observed in the initial two stories and decreases in the fourth story.
This indicates that the impact of foundation input motions on Station 4613 is more complex, with notable fluctuations in some story drifts and reductions in others.

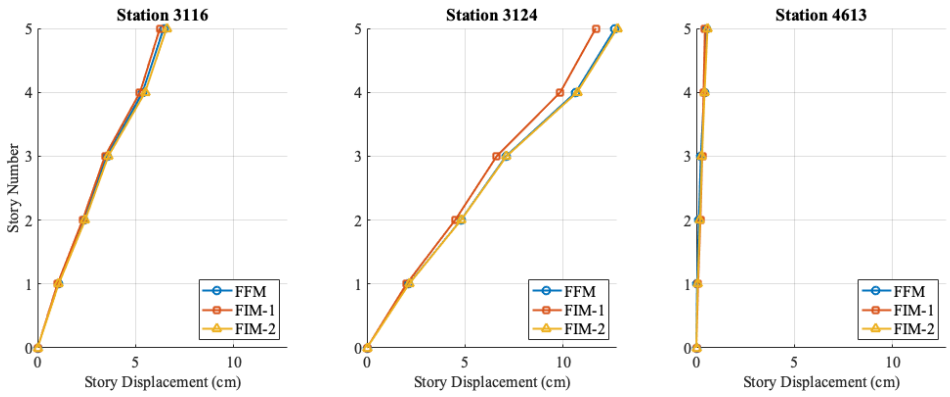

Figure 3.17. Story Displacement vs. Story Number with X-axis Limits.

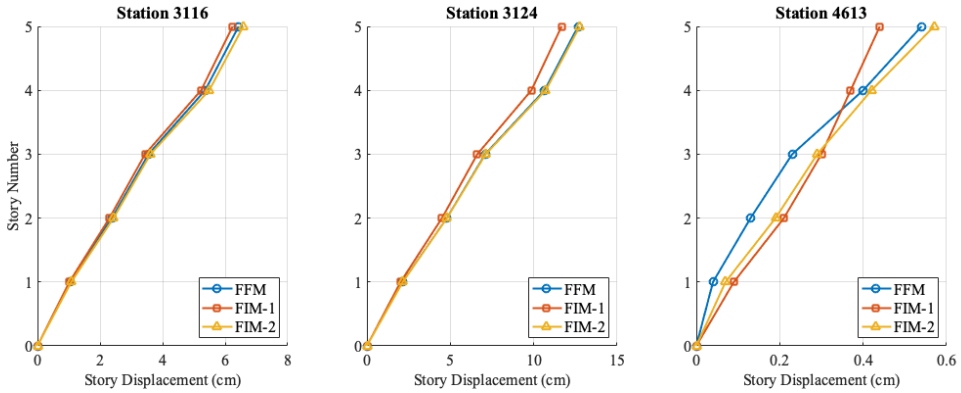

Figure 3.18. Story Displacement vs. Story Number with Full X-axis Range.

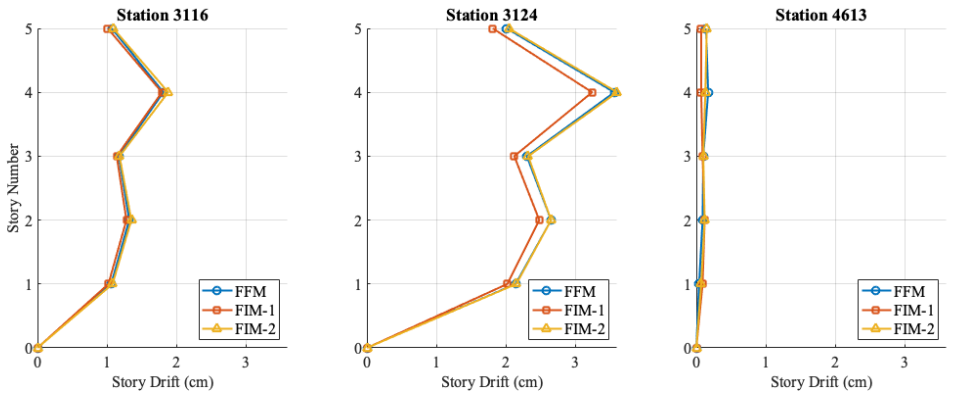

Figure 3.19. Story Drift vs. Story Number with X-axis Limits.

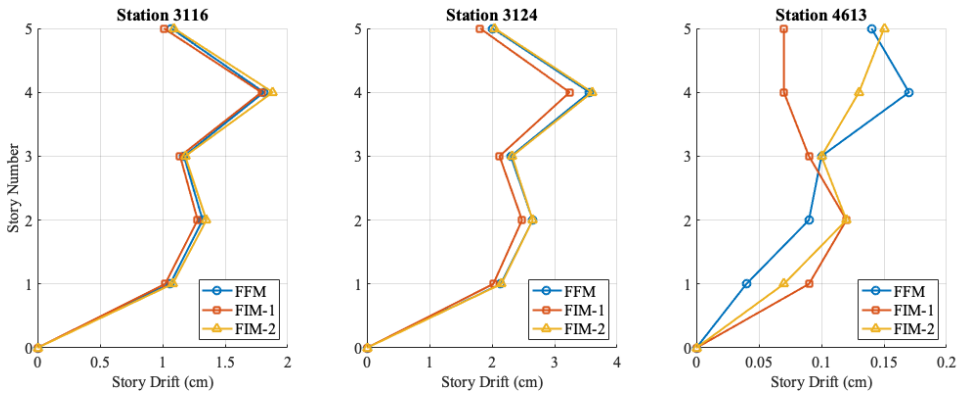

Figure 3.20. Story Drift vs. Story Number with Full X-axis Range.

In summary, Station-4613 shows the greatest variability in foundation input motions, indicating its high sensitivity due to local conditions. Stations 3116 and 3124 show high consistency across the FIMs. Overall, FIM-1 produces slightly lower displacement values than FFM and FIM-2, which might suggest a more conservative

estimate. The findings suggest that the type of foundation is a key factor in controlling the displacement and drift response, highlighting the importance of appropriate foundation design in seismic areas.

Figure 3.21 to 3.23 show the cumulative story shear and base shear plots for each case. Figure 3.21 clearly illustrates the changes in cumulative story shear at different stations, restricting the scale of the x-axis for a detailed focus on specific differences associated with FFM. Subsequently, Figure 3.22 shows the full range of cumulative story shear values for a thorough comparison between the different input motions (FFM, FIM-1, FIM-2). Figure 3.23 highlights the base shear results obtained from FFM, FIM-1, FIM-2 at three stations (Stations 3116-3124-4613), and provides a complete summary of the data. Additionally, inter-story shear values vs story numbers are given in Figure 3.24 and Figure 3.25. These results, when compared, lead to the following key findings:

(i) Station-3116: The results show that the story shear force decreases steadily as the number of stories increases, regardless of the foundation type (FFM, FIM-1, FIM-2).

FFM: Story shear values decrease from 3254.5 kN at the 1st story to 1099.1 kN at the 5th story.

FIM-1: Slightly lower values compared to FFM, ranging from 3136.1 kN to 1043.3 kN.

FIM-2: Slightly higher values than FFM, ranging from 3330.8 kN to 1127.9 kN.

The slight discrepancies in story shear between FFM, FIM-1, and FIM-2 indicate that both unfiltered and filtered motions produce comparable shear distributions for this station. The base shear values for Station-3116 are practically identical across all three motions. FFM and FIM-2 have very similar values, with FIM-1 being slightly lower, suggesting that the different foundation input motions have a minimal influence on the base shear values of this station.

(ii) Station-3124: The shear values in Station 3124 decrease as the number of stories increases, similar to the other stations.

FFM: Story shear values range from 6599.3 kN at the 1st story to 2062.1 kN at the 5th story.

FIM-1: Lower than FFM values, ranging from 6479.3 kN to 1847.4 kN.

FIM-2: Very close to FFM, ranging from 6623.6 kN to 2090.8 kN.

As with Station-3116, Station-3124 also displays minor but noticeable shear differences, indicating consistency between the free field and foundation input motions. The FIM-1 results tend to be slightly lower overall. The base shear values of Station-3124 are very close across all three motions. FIM-1 shows marginally lower values than FFM and FIM-2, suggesting that FIM-1 might provide more conservative estimates.

(iii) Station-4613: The shear values for this station remain consistently low, regardless of changes in foundation modifications.

FFM: Story shear values range from 106.392 kN at the 1st story to 155.944 kN at the 5th story, showing a slight increase at higher stories.

FIM-1: Higher variability with values ranging from 263.412 kN at the 1st story to 77.076 kN at the 5th story.

FIM-2: Values range from 215.644 kN at the 1st story to 173.348 kN at the 5th story.

This station exhibits significant differences in story shear values in relation to the type of foundation. FFM and FIM-2 have closer values, while FIM-1 deviates considerably, which may indicate sensitivity to the foundation type. Station 4613 also shows more variability in base shear values than other stations. FFM has the lowest base shear, FIM-1 the highest, with FIM-2 in the middle. This indicates that the station is particularly susceptible to changes in foundation type. On the other hand, the base shear values are relatively low due to the broadband nature of the recorded ground motion and the high V_{s30} value, which reduces shear demands.

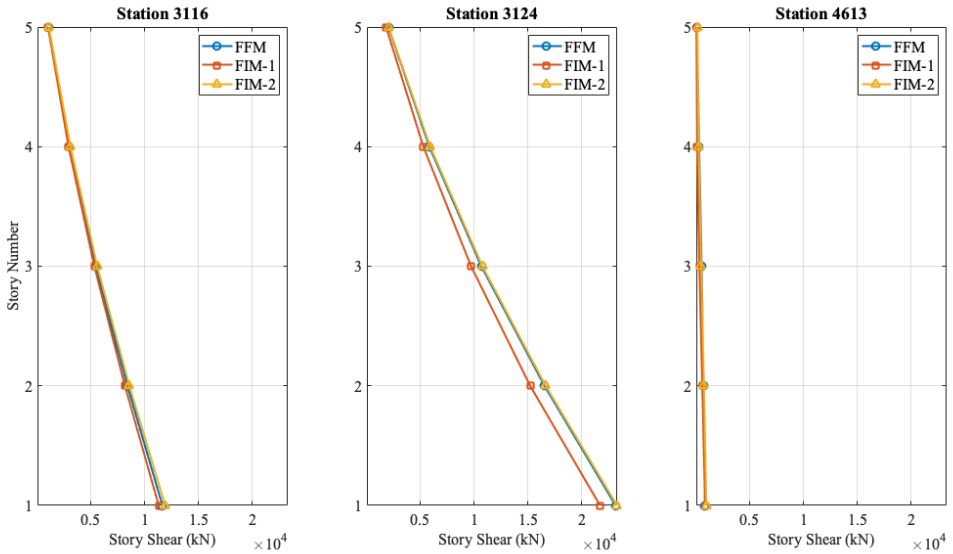

Figure 3.21. Cumulative Story Shear vs. Story Number with X-axis Limits.

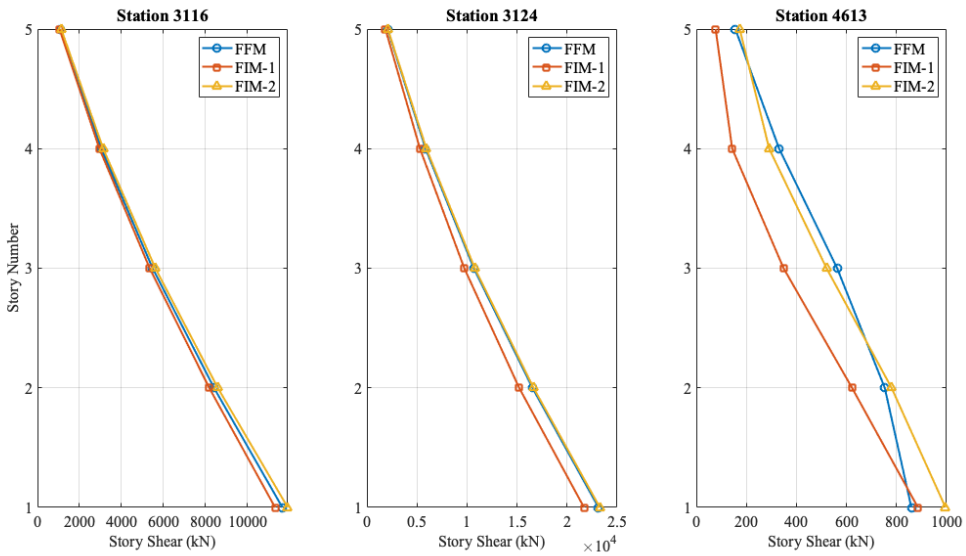

Figure 3.22. Cumulative Story Shears vs. Story Number with Full X-axis Range.

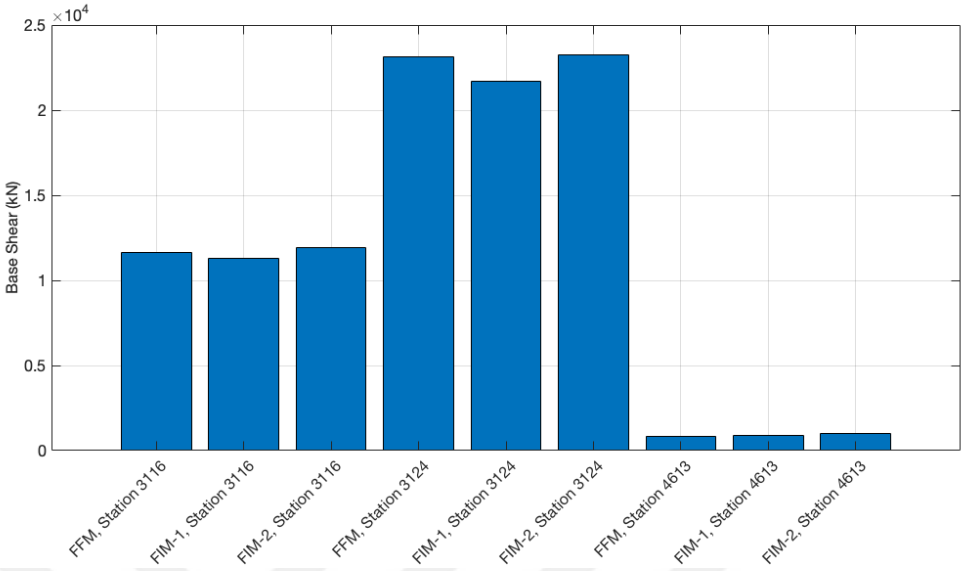

Figure 3.23. Comparison of Base Shear Values of Different Input Motions (FFM, FIM-1, FIM-2) and Stations.

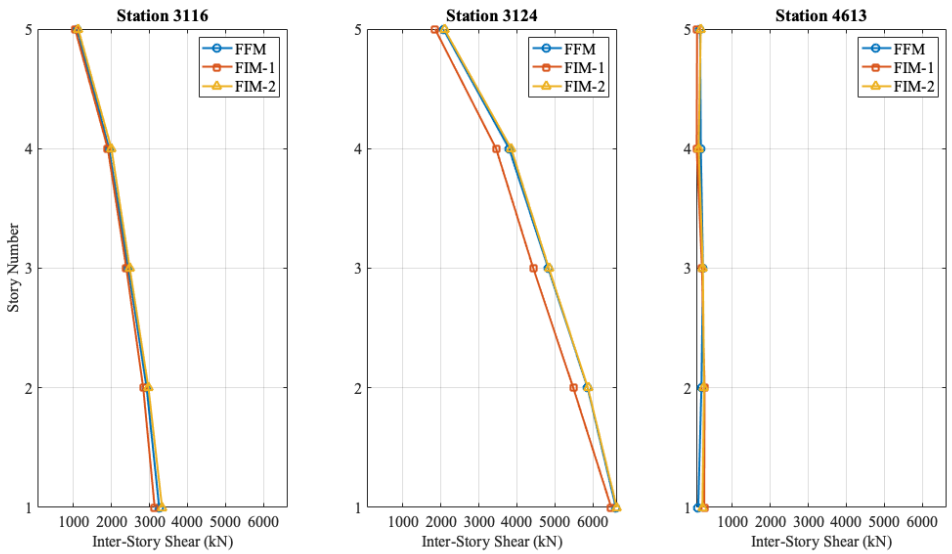

Figure 3.24. Inter - Story Shear vs. Story Number with X-axis Limits.

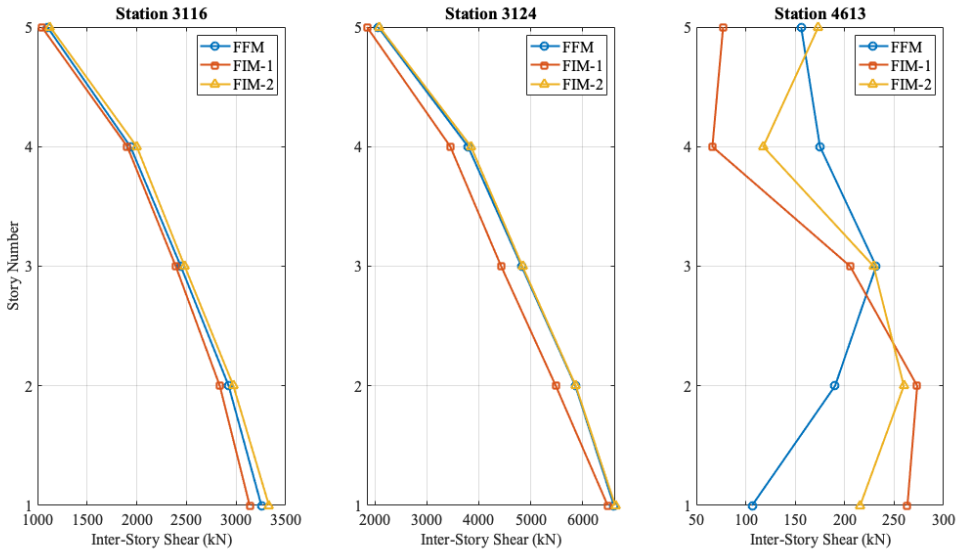

Figure 3.25. Inter - Story Shears vs. Story Numbers with Full X-axis Range.

In summary, Station-4613 exhibits the most significant variability among the different input motions (FFM, FIM-1 and FIM-2), indicating that the use of different foundation types can result in more pronounced differences in story shear results. Stations 3116 and 3124 show high consistency across the free field and foundation input motions. In general, the FIM-1 tends to provide slightly lower shear values in comparison to the FFM and FIM-2, which may suggest a more conservative estimate.

The base shear values for Stations 3116 and 3124 are relatively consistent across the different input motions, with minimal differences. This provides similar results for these stations. Additionally, the base shear values observed at Stations 3116 and 3124 are considerably higher than those observed at Station 4613. This indicates that the structural response at Stations 3116 and 3124 is much stronger, which could be due to various factors depending on the ground motion characteristics and site conditions.

The observed trend of FIM-1 providing slightly lower base shear values compared to FFM and FIM-2 is consistent across all stations, suggesting that FIM-1 may be providing a more conservative estimate in general. The observed variations for Station-4613 highlight the importance of considering kinematic SSI.

4. CONCLUSION

This thesis presents a methodology and its practical applications for incorporating the effects of kinematic Soil-Structure Interaction (SSI) on structural response. The results show the significance of foundation characteristics, including geometry, embedment depth and surrounding soil, on the seismic response of structures. For two different foundations, the frequency-dependent Foundation Impedance Functions (FIFs) are converted into time-domain filters. The optimal parameters of the filters were identified through a process of least squares approximation, which involved the minimization of error. The weighting functions were employed during this process to stabilise the filters and to alter the contribution of different frequencies. This approach yielded a strong correlation between the frequency and time domain responses in terms of amplitude and phase, with negligible deviations observed throughout the frequency range. Two foundation types (FT) were analyzed as circular surface foundations, each with a radius of 10 meters, and subjected to horizontal movement. FT-1 was located on homogeneous soil media, while FT-2 was situated on stratified soil layers, extending to a height of twice the radius (H=2R), and underlain by rigid bedrock.

The impedance function analysis reveals a number of notable patterns in the stiffness and damping coefficients for FT-1 as the dimensionless frequency increases. The stiffness coefficient shows a decrease starting at approximately 1.0 at $a_0 = 0$ and eventually stabilising at approximately 0.75 at $a_0 = 8$. This indicates that the foundation becomes increasingly flexible at higher dimensionless frequencies, suggesting a reduction in its ability to resist deformation under dynamic loading. Conversely, the damping coefficient remains relatively constant with minimal changes. When $a_0 = 0$, it commences at about 0.55, then ascends to almost 0.65 for $a_0 = 6$ and remains until $a_0 = 8$. This trend suggests a slight increase in the foundation's capacity to dissipate energy as the dimensionless frequency rises, which can help to reduce vibrations.

The FT-2 impedance function analysis indicates that there are notable changes in both the stiffness and damping coefficients as the dimensionless frequency rises. The stiffness coefficient displays a fluctuating downward trend. Initially, the stiffness coefficient is approximately 1.0 at $a_0 = 0$, dropping to around 0.67 at $a_0 = 1$, and then fluctuating between 1.1 to 0.2, before stabilising at approximately 0.4 at $a_0 = 6$. This fluctuating trend suggests that the foundation's stiffness resists deformation under dynamic loading to varying degrees, influenced by frequency and soil layering. Conversely, the damping coefficient demonstrates an increasing and fluctuating trend. Initially, at $a_0 = 0$, the coefficient is approximately 0.1, but as a_0 increases to 1, it rises to approximately 0.6. Between $a_0 = 1$ and $a_0 = 6$, the coefficient fluctuates between 0.5 and 0.88. This indicates a complex interaction between the foundation and the surrounding soil layers. The foundation's capacity to dissipate energy improves with higher dimensionless frequencies, although this is also influenced by the kinematic soil-structure interaction effects.

The impedance function analysis of the FTs considered provides critical insight into the dynamic response of the foundations. The impedance functions related to FT-1 demonstrate a consistent increase in amplitude with rising frequency. The initial value of amplitude is around 1.0 at 0 Hz and gradually climbs to 1.35 at 10 Hz, 2.15 at 20 Hz, 3.0 at 30 Hz, 4.0 at 40 Hz, and 5.0 at 50 Hz. This pattern indicates a more pronounced dynamic response from the foundation at higher frequencies, which is consistent with the observed decrease in stiffness. In addition, phase analysis indicates that the impedance function's phase response increases with frequency. Initially, at 0 Hz, the phase response was rapidly increased to approximately 0.77 radians at 10 Hz, 1.1 at 20 Hz, 1.3 at 30 Hz, 1.4 at 40 Hz, and approximately 1.5 at 50 Hz. This rising phase response indicates a delay in the system's response to dynamic loading with increasing frequency.

The impedance functions related to FT-2 exhibit an overall increase in frequency, interrupted, with some irregular fluctuations observed. The amplitude is approximately 1.0 at 0 Hz, representing the initial foundation response. As the frequency increases, the

amplitude follows, reaching approximately 1.2 at 2 Hz, 1.3 at 4 Hz, 2.8 at 6 Hz, 4.0 at 8 Hz, and 5.5 at 10 Hz. The complex dynamic response of the foundation, influenced by the layered soil media, is indicated by multiple peaks and drops. Despite the observed variations, the overall rise in amplitude implies that the foundation's dynamic response is more significant at higher frequencies. Additionally, the FT-2 phase analysis reveals a complex pattern in impedance functions. The phase starts at about 0.1 radians at 0 Hz and then rises sharply to 0.8 radians at 2 Hz, reaching approximately 1.2 radians at 4 Hz. It then stabilises around 1.65 radians at 10 Hz, with minor changes. This variable phase response indicates a changing delay in the system's response to dynamic loading with increasing frequency, reflecting complex interactions between the foundation and surrounding soil layers.

The findings are consistent in both the frequency domain and the time domain obtained by transforming discrete-time recursive filters. They provide valuable information about considering kinematic SSI. Furthermore, free field motion (FFM) frequency content changes the influence of foundation input motions.

This thesis considered five types of FFM time histories: two simulated ones (Ricker wavelets) and three real earthquake records (recorded at the three stations, Stations 3116-3124-4613, during the 6 February 2023 Kahramanmaraş Earthquake). Real earthquake records, and their filtered motions (FIM-1 and FIM-2) were applied to a five-story model of a symmetrical building. The analysis results show that Stations 3116 and 3124 are relatively consistent across the different input motions (FFM, FIM-1, FIM-2), with minimal differences, resulting in similar structural responses for these stations. Additionally, the structural response at these stations is much stronger than Station-4613 due to their specific ground motion characteristics and site conditions. The observed trend of FIM-1 provides a slightly lower structural response than FFM and FIM-2, suggesting a more conservative estimate.

The study found that FT has a critical effect on structural response, especially for short-period structures, highlighting the importance of proper foundation design in

seismic areas. The research offers valuable insights into the behavior and performance of structures subjected to kinematic SSI and provides a simple technique to incorporate frequency-dependent impedance functions in time-domain structural analysis software.

REFERENCES

1. Veletsos, A. S. and J. W. Meek, "Dynamic behaviour of building-foundation systems", *Earthquake Engineering & Structural Dynamics*, Vol. 3, No. 2, pp. 121–138, 1974.

2. Youssef, A., *Seismic Response of Inelastic Structures on Compliant Foundations*, Ph.D. Thesis, Northeastern University, 1998.

3. Mohammed-Eltaher, A. H., *Hybrid FE-BE Formulation for Coupled Dynamic Poroelastoplastic Analysis of Soil-Structure Systems*, Ph.D. Thesis, Rice University, 1999.

4. Wolf, J., *Dynamic Soil-Structure Interaction*, Prentice Hall, New Jersey, 1985.

5. Zaicenco, A. and V. Alkaz, "Soil-Structure Interaction Effects on an Instrumented Building", *Bulletin of Earthquake Engineering*, Vol. 5, pp. 533–547, 2007.

6. Lee, W. V., "Effect of Foundation Embedment on Soil-Structure Interaction", *The 7th World Conference on Earthquake Engineering*, Istanbul, Turkiye, pp. 225–228, 1980.

7. Lin, N. A., "Measured Effect of Foundation Embedment on Response", *The 8th World Conference on Earthquake Engineering*, San Francisco, USA, pp. 841–847, 1984.

8. Inoue, Y. and M. Kawano, "Dynamic Response of an Elastic Foundation Embedded in a Layered Medium", *The 8th World Conference on Earthquake Engineering*, San Francisco, USA, pp. 753–759, 1984.

9. Avilés, J. and L. E. Pérez-Rocha, "Effects of Foundation Embedment During Building–Soil Interaction", *Earthquake Engineering & Structural dynamics*,

Vol. 27, No. 12, pp. 1523–1540, 1998.

10. Apsel, R. and J. Luco, "Impedance Functions for Foundations Embedded in a Layered Medium: An Integral Equation Approach", *Earthquake Engineering & Structural Dynamics*, Vol. 15, No. 2, pp. 213–231, 1987.

11. Luco, J. E. and H. L. Wong, "Seismic Response of Foundations Embedded in a Layered Half-Space", *Earthquake Engineering & Structural dynamics*, Vol. 15, No. 2, pp. 233–247, 1987.

12. Wong, H. L. and J. E. Luco, *Tables of Impedance Functions and Input Motions for Rectangular Foundations*, University of California, Department of Civil Engineering, 1978.

13. Dobry, R. and G. Gazetas, "Dynamic Response of Arbitrarily Shaped Foundations", *Journal of Geotechnical Engineering*, Vol. 112, No. 2, pp. 109–135, 1986.

14. Gazetas, G. and J. L. Tassoulas, "Horizontal Damping of Arbitrarily Shaped Embedded Foundations", *Journal of Geotechnical Engineering*, Vol. 113, No. 5, pp. 458–475, 1987.

15. Gazetas, G. and J. L. Tassoulas, "Horizontal Stiffness of Arbitrarily Shaped Embedded Foundations", *Journal of Geotechnical Engineering*, Vol. 113, No. 5, pp. 440–457, 1987.

16. Novak, M. and L. El Hifnawy, "Effect of Foundation Flexibility on Dynamic Behaviour of Buildings", *The 8th World Conference on Earthquake Engineering*, San Francisco, USA, pp. 721–727, 1984.

17. Ambrosini, R. D., J. D. Riera and R. F. Danesi, "On the Influence of Foundation Flexibility on the Seismic Response of Structures", *Computers and Geotechnics*, Vol. 27, No. 3, pp. 179–197, 2000.

18. Hadjian, A. H., J. E. Luco and N. C. Tsai, "Soil-Structure Interaction: Continuum or Finite Element?", *Nuclear Engineering and Design*, Vol. 31, No. 2, pp. 151–167, 1974.

19. Luco, J., A. Hadjian and H. Bos, "The Dynamic Modeling of the Half-Plane by Finite Elements", *Nuclear Engineering and Design*, Vol. 31, No. 2, pp. 184–194, 1974.

20. Yang, Z., *Numerical Modeling of Earthquake Site Response Including Dilation and Liquefaction*, Ph.D. Thesis, Columbia University, 1999.

21. Shakib, H., "Evaluation of Dynamic Eccentricity by Considering Soil–Structure Interaction: A Proposal for Seismic Design Codes", *Soil Dynamics and Earthquake Engineering*, Vol. 24, No. 5, pp. 369–378, 2004.

22. Shakib, H. and A. Fuladgar, "Dynamic Soil–Structure Interaction Effects on the Seismic Response of Asymmetric Buildings", *Soil Dynamics and Earthquake Engineering*, Vol. 24, No. 5, pp. 379–388, 2004.

23. Seunghyun, K., *Calibration of simple models for seismic soil-structure interaction from field performance data*, Ph.D. Thesis, University of California, Los Angeles, 2001.

24. Villaverde, R., *Fundamental Concepts of Earthquake Engineering*, CRC press, Boca Raton, 2009.

25. Gcr, N., "Soil-Structure Interaction for Building Structures", *National Institute of Standards and Technology (NEHRP)*, 2012.

26. Veletsos, A. S. and V. D. Nair, "Seismic Interaction of Structures on Hysteretic Foundations", *Journal of the Structural Division*, Vol. 101, No. 1, pp. 109–129, 1975.

27. *NEHRP Recommended Provisions (National Earthquake Hazards Reduction Program) for Seismic Regulations for New Buildings and Other Structures*, Tech. rep., National Earthquake Hazards Reduction Program (US) and Building Seismic Safety Council (US), 2001.

28. Stewart, J. P., G. L. Fenves and R. B. Seed, "Seismic Soil-Structure Interaction in Buildings. I: Analytical Methods", *Journal of Geotechnical and Geoenvironmental Engineering*, Vol. 125, No. 1, pp. 26–37, 1999.

29. Worku, A., "Soil-Structure Interaction Provisions-A Potential Tool to Consider for Economical Seismic Design of Buildings?", *Journal of the South African Institution of Civil Engineering*, Vol. 56, No. 1, pp. 54–62, 2014.

30. Mylonakis, G. and G. Gazetas, "Seismic Soil-Structure Interaction: Beneficial or Detrimental?", *Journal of Earthquake Engineering*, Vol. 4, No. 3, pp. 277–301, 2000.

31. Kramer, S. L., *Geotechnical Earthquake Engineering*, Prentice Hall, New Jersey, 1996.

32. Şafak, E., "Time-Domain Representation of Frequency-Dependent Foundation Impedance Functions", *Soil Dynamics and Earthquake Engineering*, Vol. 26, No. 1, pp. 65–70, 2006.

33. Wolf, J. P. and M. Motosaka, "Recursive Evaluation of Interaction Forces of Unbounded Soil in the Time Domain From Dynamic-Stiffness Coefficients in the Frequency Domain", *Earthquake Engineering & Structural Dynamics*, Vol. 18, No. 3, pp. 365–376, 1989.

34. Laudon, A. D., O.-S. Kwon and A. R. Ghaemmaghami, "Stability of the Time-Domain Analysis Method Including a Frequency-Dependent Soil–Foundation System", *Earthquake Engineering & Structural Dynamics*, Vol. 44, No. 15, pp. 2737–

2754, 2015.

35. Gash, R., E. E. Seylabi and E. Taciroglu, "Implementation and Stability Analysis of Discrete-Time Filters for Approximating Frequency-Dependent Impedance Functions in the Time Domain", *Soil Dynamics and Earthquake Engineering*, Vol. 94, pp. 223–233, 2017.

36. Tang, Z., X. Li and Z. Wang, "Stable Parameters Identification for Rational Approximation of Single Degree of Freedom Frequency Response Function of Semi-Infinite Medium", *International Journal for Numerical Methods in Engineering*, Vol. 124, No. 24, pp. 5596–5615, 2023.

37. Sung, Y.-C. and C.-C. Chen, "Z-Transferred Discrete-Time Infinite Impulse Response Filter as Foundation–Soil Impedance Function for SDOF Dynamic Structural Response Considering Soil–Structure Interaction", *Earthquake Spectra*, Vol. 35, No. 2, pp. 1003–1022, 2019.

38. Şafak, E., "Discrete-Time Analysis of Seismic Site Amplification", *Journal of Engineering Mechanics*, Vol. 121, No. 7, pp. 801–809, 1995.

39. Şafak, E., *Analysis of Recordings in Structural Engineering; Adaptive Filtering, Prediction, and Control*, Tech. rep., US Geological Survey, 1988.

40. Oppenheim, A. V., *Discrete-Time Signal Processing*, Pearson Education, 1999.

41. Levy, E. C., "Complex-Curve Fitting", *IRE Transactions on Automatic Control*, Vol. AC-4, No. 1, pp. 37–43, 1959.

42. Pearson, K. and J. Blakeman, *Mathematical Contributions to the Theory of Evolution. XIII. On the Theory of Contingency and Its Relation to Association and Normal Correlation*, Dulau and Co., London, 1904.

43. "MATLAB Version:12.6.2 (R2023b)", http://www.mathworks.com.

44. Sieffert, J. G. and F. Cevaer, *Handbook of Impedance Functions*, Ouest Editions, Nantes, 1992.

45. Ricker, N., "The Form and Laws of Propagation of Seismic Wavelets", *Geophysics*, Vol. 18, No. 1, pp. 10–40, 1953.

46. AFAD, "1900 – 2023 Earthquake Catalog (M $\geq$ 4.0)", , 2023, `https://deprem.afad.gov.tr/depremkatalogu`, accessed on April 13, 2023.

47. TADAS-AFAD, "Republic of Turkiye Prime Ministry Disaster & Emergency Management Authority (AFAD)", 2023, `tadas.afad.gov.tr`, accessed on April 13, 2023.

48. Malhotra, P. K., *Seismic Analysis of Structures and Equipment*, Springer, Sharon, 2021.

49. Veletsos, A. S. and Y. T. Wei, "Lateral and Rocking Vibration of Footings", *Journal of the Soil Mechanics and Foundations Division*, Vol. 97, No. 9, pp. 1227–1248, 1971.

50. Kausel, E., *Forced Vibrations of Circular Foundations on Layered Media*, Tech. rep., Massachusetts Institute of Technology, 1974.

51. Luco, J. E. and R. A. Westmann, "Dynamic Response of Circular Footings", *Journal of the Engineering Mechanics Division*, Vol. 97, No. 5, pp. 1381–1395, 1971.

52. Newmark, N. M., "A Method of Computation for Structural Dynamics", *Journal of the Engineering Mechanics Division*, Vol. 85, No. 3, pp. 67–94, 1959.

53. Karakaya, M., *Betonarme Taşıyıcı Sistemlerin Doğrusal Olmayan Yöntemlerle Performansının Değerlendirilmesi*, Master's Thesis, Istanbul Technical University, 2013.